5-2018

A novel design for a silicon and cadmium telluride tandem solar cell.

Jacob A Vittitow
University of Louisville
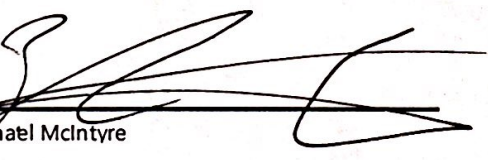
A Novel Design for a Cadmium Telluride-Silicon Tandem Solar Cell
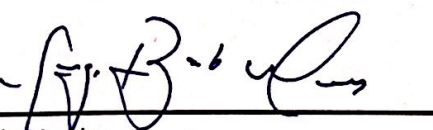
Submitted by: X _____

Jacob Vittilow

A Thesis Approved on April 23rd, 2018 by the following Reading and Examination Committee:

X _____

Shamus McNamara
Thesis Director

X _____

Michael McIntyre

X _____

Sergio Mendes

A Novel Design for a Cadmium Telluride and Silicon Tandem Solar Cell

Jacob Vittitow, University of Louisville J.B. Speed School of Engineering –

Department of Electrical and Computer Engineering

Thesis Advisor: Dr. Shamus McNamara

April 9, 2018

1. Introduction

According to the U.S. Department of Energy, from 2008 to 2018, the amount of solar energy sources connected to the American Bulk Power System (BPS) increased by a factor of twenty, driven by increasing efficiencies of individual photovoltaic cells and reduced material costs [1]. However, challenges to solar energy increasing its prevalence in the American generation portfolio are still being addressed; primary among these is the need for further increased efficiencies to be competitive with fossil fuel generation on a cost-per-kilowatt-hour basis. At the time of writing, the U.S. Department of Energy estimates the cost of solar energy at the utility scale to be approximately $0.12/kWh, with the goal to be competitive with more traditional power generation set at $0.06/kWh [2]. As of 2018, EnergySage reports that the most efficient commercially-available solar cells are rated at an efficiency of 22.5%, with most cells rated between 14% and 16% [3].

Based upon first quarter 2017 statistics published by the National Renewable Energy Laboratory, the average cost of a PV module to the consumer is $0.65/W for an industrial installation and $0.73/W for domestic installations [21]. The cost breakdown is shown in Figure 1 below.
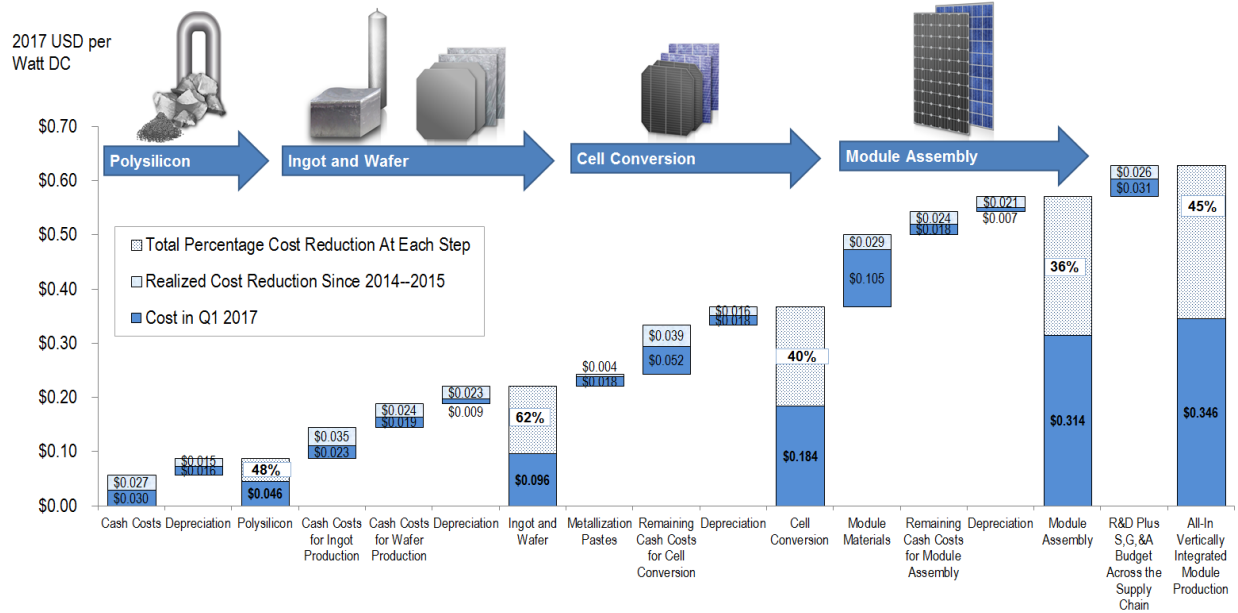
Figure 1 - NREL Cost Breakdown for a standard PV module [21]

Based upon these cost estimates and an assumed average nominal solar cell efficiency of 16.2%, it is possible to establish a cost versus efficiency relationship that illustrates how vital cell efficiency is from an economic perspective. Figure 2 depicts the relationship between increasing cell efficiency and decreasing cost on a per-Watt basis. As illustrated in Figure 2, nominal efficiencies in excess of 20% represent a significant financial improvement over modern standard efficiencies. One widely accepted solar cell design architecture that can be used to achieve these high cell efficiencies is the tandem cell design.
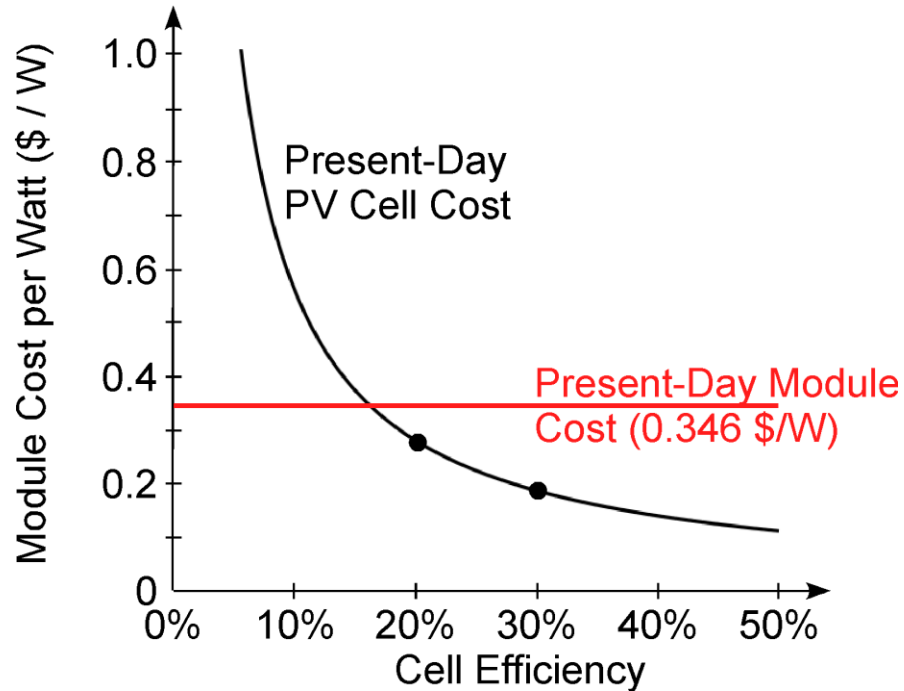
Figure 2 - Relationship between cost per watt of a PV module and increasing nominal efficiencies [21]
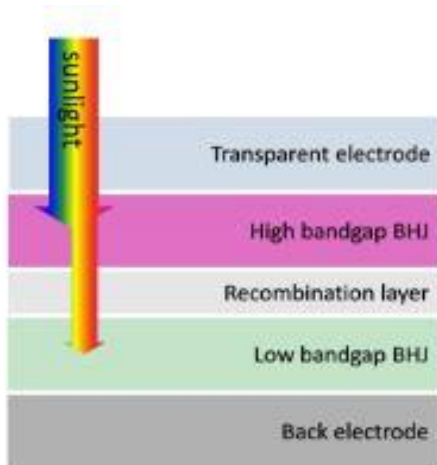
Figure 3 - Generic depiction of a Tandem Solar Cell, depicting the interactions between different solar radiation frequencies and the absorber layers [4].

The tandem solar cell design scheme has been recognized for years as a method of utilizing semiconductor materials of varying bandgap energies to absorb a larger wavelength spectrum of available solar radiation than a single semiconductor material is capable of. Figure 3 explains some of the operational principles of tandem solar cells, the most fundamental being that the top absorber layer consists of a larger bandgap semiconductor material that absorbs high frequency solar radiation and a smaller bandgap semiconductor material in the bottom layer that absorbs low frequency solar radiation. By utilizing the differing materials, a larger portion of the

4

available solar radiation can be absorbed and less waste heat will be produced by unabsorbed radiation, resulting in a significantly higher overall conversion efficiency. Tandem solar cells can be constructed as 2-terminal devices, as shown in Figure 1, or with each cell electrically separated and with its own set of terminals. This paper will present a novel design for a tandem solar cell that utilizes a cadmium telluride (CdTe) absorber in the top cell and a more traditional silicon cell as the substrate and a four-terminal tandem cell architecture, where each absorber layer is mechanically stacked but electrically separated with its own anode and cathode to allow for separate optimization that doesn't require identical current through the cells. This design achieves conversion efficiencies exceeding 27% in TCAD simulation.

2. Background
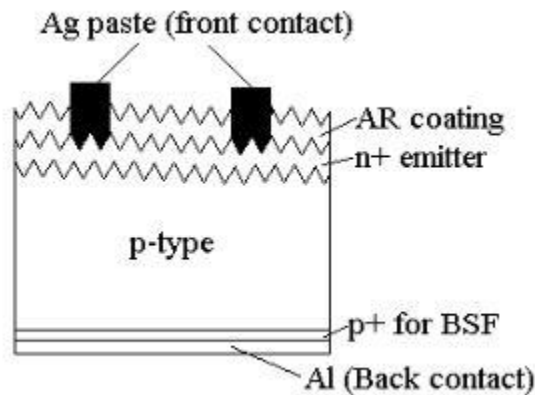
Figure 4 - Schematic of a Commercially Available Multicrystalline Silicon Solar Cell of the early 2010's [7].

The first multi-junction solar cell was developed in 1979, utilizing an AlGaAs junction and a GaAs junction, interconnected with an epitaxially grown tunnel junction [5]. Subsequent designs utilizing the same conceptual template were developed throughout the 1990's and the 2000's, utilized mostly for space applications because of the incredibly high cost of production of the semiconductor materials used in the cells. The research focus on multijunction cells that used lower cost materials, primarily silicon, came about in the 1980's and early 1990's. The first notable example of a silicon heterojunction solar cell, utilizing amorphous (a-Si) and polycrystalline silicon (p-Si), was developed by a team at Osaka University in 1981. Their cell was developed by increasing the carbon content of amorphous silicon during the plasma-

deposition process, increasing the bandgap energy of the silicon above that of polycrystalline silicon [6]. When stacked to form a p-n junction, the a-Si/p-Si structure demonstrated a conversion efficiency of 7.1%, which was a major improvement over previous efforts of the 1970's. By 2004, advancements in fabrication techniques had driven the maximum demonstrated efficiency of silicon heterojunction solar cells to 20.4% [7].

Much research has also been done in the field of tandem solar cells utilizing different semiconductor materials, matched according to their bandgap energies. The earliest tandem solar cell designs were published in the mid 1970's, many of them utilizing AlGaAs absorbers, which are expensive to produce [8]. Early tandem solar cells were demonstrated with efficiencies as high as 30%, but utilizing materials far too costly to be economical at industrial scale. In the last ten years, research has shifted to focus on producing solar cell designs with demonstrably higher efficiencies than single junction cells that utilize progressively thinner and less expensive absorber layers to improve the economy at commercial scale. There has also been a noted shift to utilizing silicon as a substrate material instead of the more costly and less mechanically robust germanium and gallium-arsenide (GaAs) substrates of laboratory tandem solar cells to allow them to be more cost-competitive with single-junction silicon cells [9].

It is in this context that the proposed design for a Cadmium Telluride (CdTe)/Silicon (Si) tandem solar cell is introduced. The first published instance of a CdTe/Si tandem cell was reported in the *IEEE Journal of Photovoltaics, Volume 7* in November 2017 [10]. In their study, the authors identified two conditions necessary for a tandem solar cell to be economically competitive with single-junction silicon cells:

1) The tandem cell must have an efficiency exceeding 25% to offset the increased material costs.

2) The two sub-cells should be roughly equal in cost, performance and reliability to justify the use of the tandem structure over separate cells.

Their tandem cell design produced a range of efficiencies from 25.8% to 27.7%, depending primarily upon the minority carrier lifetime assumed in the CdTe absorber. The cell utilized a four-wire architecture, where each sub-cell had an independent anode and cathode. All simulations were carried out in Sentaurus Device software package, assuming the illumination of a standard AM1.5G spectrum and an ambient temperature of 300K ($27^{\circ C}$).

3. Methods and Design

The first decision made in the design was choosing the compound semiconductor material from the III/V group or the II/VI group that would be well-matched to the silicon bandgap of 1.08 eV for light absorption purposes. Silicon was specified as the substrate material because it is cost-effective and can be manufactured with incredibly low defect densities, reducing carrier recombination rate. Silicon is also an indirect bandgap semiconductor, which contributes to longer charge

Figure 5 - Binary Semiconductor Materials Arranged by Bandgap Energy (eV) and Lattice constant (nm) [11]

7

carrier lifetimes and lower recombination rates [12]. Figure 5 shows a variety of III/V binary semiconductors and II/VI compound semiconductors and their bandgap energies and lattice constants. In heterojunction designs, it is necessary to match lattice constants closely to reduce mechanical strain at the interfaces between differing materials and reduce interface recombination effects [12]. However, in this design, the silicon sub-cell and the binary semiconductor sub-cell are mechanically separated by a transparent conducting oxide (TCO). This allows the binary semiconductor to be chosen on the basis of bandgap energy and optoelectronic properties. CdTe was selected as the binary material because its bandgap of 1.48 eV is well suited to absorption of light in the visible spectrum, which is an area of high intensity for solar radiation. It also has incredibly low absorption lengths in the visible spectrum [13], allowing the layers to be optically thin (on the order of 100 nm thick), reducing production cost and time.

The second design consideration was the transparent conducting oxide (TCO) that would be used as the front contact material, as well as the mechanical separator for the two sub-cells of the tandem structure. The requirements that the material had to fulfill were:

1) It had to allow a majority of light in the 300 nm to 1100 nm range to transmit with little absorption to adhere to the bandgap energies of silicon and CdTe.

2) It had to be capable of being either conductive or insulating, based upon the doping profile.

3) It had to be chemically inert when in contact with both CdTe and silicon to preserve the possible lifetime of the solar cell.

Zinc Oxide (ZnO) was chosen as the TCO material because its bandgap (3.1 eV) is wide enough to transmit light with longer wavelengths than approximately 280 nm with approximately 90% transmittance. ZnO is a direct bandgap semiconductor with a variety of intrinsic defects (Zn vacancies, interstitial Zn atoms, and interstitial O atoms) that make it inherently a poor conductor [14]. However, it readily accepts dopant atoms, such as aluminum, which give it

Figure 6 - Transmittance spectrum of ZnO thin films doped with aluminum at different processing temperatures [14]

favorable optical and electronic properties for transparent ohmic contacts with other semiconductor materials. Figure 6 shows the transmittance percent of aluminum-doped zinc oxide thin films at different annealing temperatures. ZnO has favorable transmission in the required spectrum and can be processed at low temperatures, reducing the possibility of "thermal donors" aggregating in the silicon substrate during processing.

The tandem solar cell was constructed and simulated using the Atlas simulation package of the *Silvaco* TCAD software. Atlas has a well-defined set of physical differential equations that it solves to determine parameters such as photogeneration rate, recombination rate (both Shockley-Read-Hall and Auger recombination), current density, charge density, and optical intensity of light through the cell. Once the material regions of the cell are specified, Atlas can simulate the photovoltaic action of charge carriers in each region and at each junction and electrode based upon dopant atoms used, dopant concentration, carrier lifetimes and optical intensity at each pre-defined mesh point. *Silvaco* also utilizes "extract" statements which can be

programmed to determine the standard parameters used to evaluate the performance of a solar cell:

1. Short-circuit current (I_{SC})

2. Open-circuit voltage (V_{OC})

3. Maximum power output (P_{max})

4. Fill factor (FF) $= \dfrac{I_{SC} * V_{OC}}{P_{max}}$ – Fill Factor is determined to define the "squareness" of the IV curve, which is an indication of the impact of the series resistance on the overall conversion efficiency.

5. Overall conversion efficiency (η)

In order to determine the efficiency of the tandem cell, a standard illumination profile must be selected for the simulation that allows the results to be directly compared to other cell nominal values. The Air-Mass-Global 1.5 (AM1.5) spectrum was selected because it is defined by the American Society for Testing and Materials (ASTM) as being a reasonable estimate for the average solar irradiance of the contiguous United States [15]. The intensity of the AM 1.5 Spectrum defined in the Atlas simulation package is shown in Figure 7 as a function of the wavelengths of solar radiation.
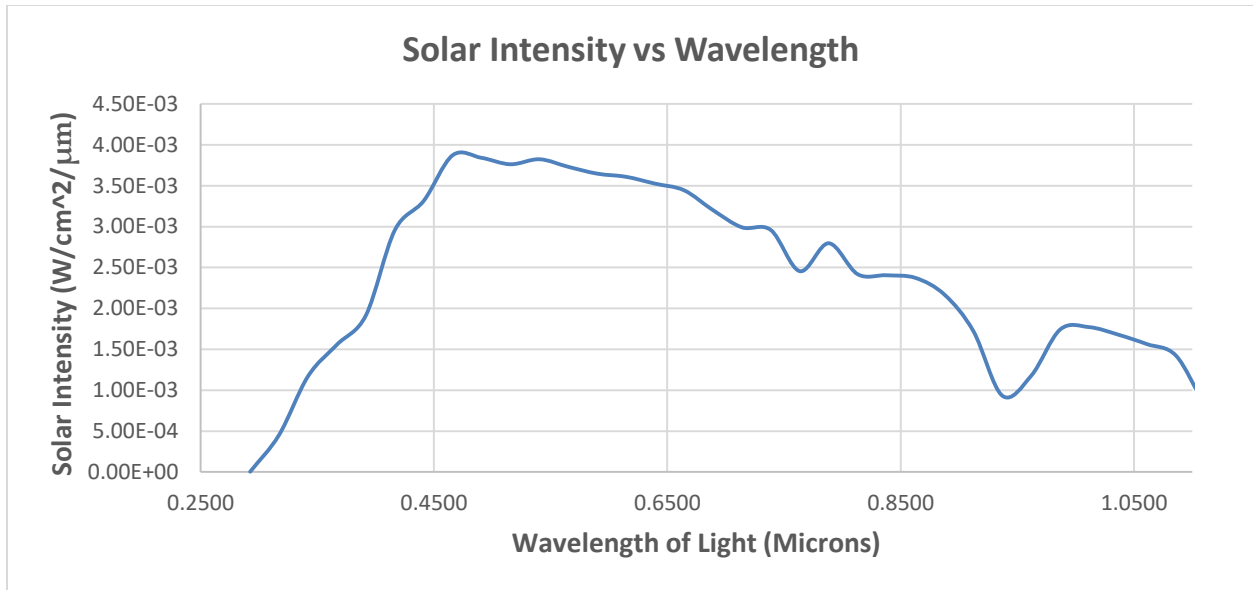
Figure 7 - AM1.5 Solar Spectrum as defined in the Atlas simulation package

In order to temper expectations about the performance of the CdTe and Si regions of the tandem cell, it is important to calculate the theoretical "maximum" wavelength of light that can be absorbed by each material, based upon its bandgap energy. This relationship is approximated by the equation [16]:

$$\lambda = \frac{1.24}{E_g} \ [\mu m]$$

λ is defined as the wavelength of the incident photon and E_g is the bandgap energy of the semiconductor material in eV. By solving this relation based upon bandgap energies of 1.49 eV and 1.08 eV, respectively, for CdTe and Si, it can be determined that CdTe will effectively absorb light with wavelengths shorter than 832 nm and Si will effectively absorb light with wavelengths shorter than 1148 nm. The average of the integrated intensities of the wavelengths below 832 nm (CdTe range) is 278 mW/cm^2, whereas the average of the integrated intensities of

the wavelengths from 832 nm to 1050 nm (Si range) is 170 mW/cm^2. Integrating the solar

intensity curve over the CdTe range yields 65.96% of the total available solar intensity, while

integrating over the Si range yields 11.71% of the total available solar intensity. This suggests

that the CdTe layer should absorb approximately 5/6 of the total available energy.

Also important to consider is the available photocurrent over the wavelength ranges of

the CdTe and Si layers. Integrating the photocurrent profile, shown in Figure 8, defined by the

AM1.5 spectrum in Atlas yields that 48.82% of all available photocurrent lies in the range of

wavelengths absorbed by the CdTe, while only 13.69% lies in the range absorbed by Si.
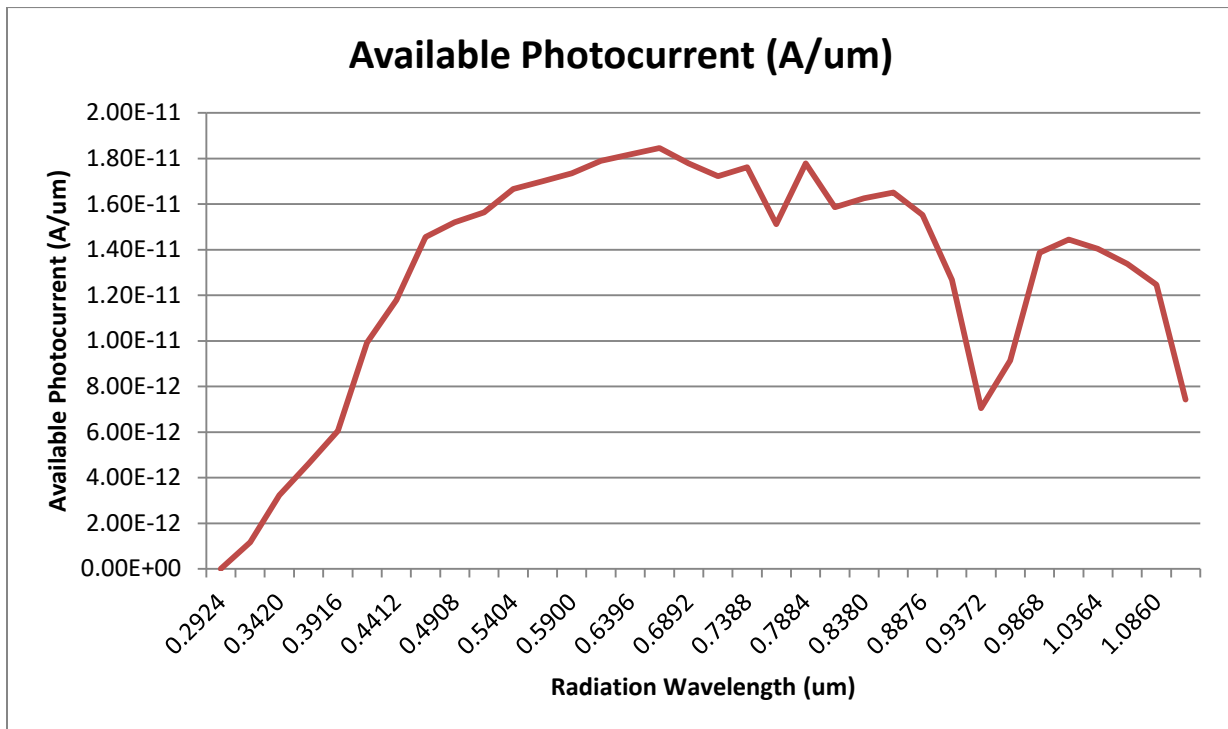
Figure 8 - Available photocurrent by wavelength in Atlas' AM1.5 spectrum

The discrepancies in optical intensity and available photocurrent in the absorption ranges

of CdTe and Si suggest that even though the CdTe layer makes up a significantly smaller portion

of the solar cell, it will account for the majority of the overall cell conversion efficiency.

The final decisions to be made in the design of the absorber layers were the doping concentrations of each absorber and the thicknesses of the absorbers. To determine the thickness of the CdTe and Si absorber layers, an analysis was performed that weighed the carrier lifetimes in each region against the minimum thicknesses required for efficient light absorption and the diffusion lengths of the charge carriers in the materials. The chosen thickness of the CdTe layer is more arbitrary than the thickness of the Si layer because it can be made optically thin and still absorb a significant portion of light in the visible spectrum [10], which greatly reduces the effects of bulk resistance and recombination losses. The thickness of the CdTe absorber layers was fixed at 100 nm thick in both the p-region and in the n-region, and then the doping concentrations were varied to allow the p-n junction depletion region to encompass the entire thickness of the CdTe layers. This would maximize V_{OC} and I_{SC} by minimizing recombination losses. The width of a p-n junction depletion region is governed by the equation [16]:

$$W_D = \sqrt{\frac{2\varepsilon_S \varepsilon_0}{q} \left(\frac{N_D + N_A}{N_D N_A}\right)(V_{bi} - V_{app})}$$

Where ε_s is the relative dielectric constant of the absorber material, ε_0 is the permittivity of free space, q is the charge of an electron, N_D and N_A are the donor and acceptor atom doping concentrations, V_{bi} is the built-in potential of the junction and V_{app} is the applied voltage. The built-in voltage is determined using the equation [16]:

$$V_{bi} = \frac{k_B T}{q} \ln\left(\frac{N_A N_D}{n_i^2}\right)$$

Where k_B is the Boltzmann constant, T is the temperature of the junction in Kelvin, and n_i is the intrinsic carrier concentration of the semiconductor material.

By solving these two relations for a desired depletion region width of 200 nm at a temperature of 300K and factoring in minor changes in V_{OC} calculated in the Atlas simulation, doping concentrations of $N_A = N_D = 10^{15}$ cm^{-3} were determined for the n-type and p-type CdTe absorbers. For simulation purposes, it was also necessary to calculate the charge carrier lifetimes in the CdTe regions. The carrier lifetimes in CdTe can be determined using the relation [13]:

$$\tau_R = \frac{1}{Bp}$$

Where B is the radiative recombination coefficient (estimated as 3 x 10^{-9} cm^3/s) and p is the doping concentration, regardless of whether the dopant atoms are donors or acceptors. Utilizing this relationship, the carrier lifetimes in both CdTe absorbers were calculated to be 333 ns.

The thickness of the Si substrate required more careful consideration. Absorption lengths of light through silicon are dependent upon the wavelength of the light, as shown in Table 1.

Also important to consider when sizing the silicon substrate are the diffusion lengths of the charge carriers and the carrier lifetimes. The diffusion lengths of charge carriers in silicon are given by the equations [16]:

λ (nm)	Absorption length in Si (μm)
300	0.0015
400	0.1
500	1.0
600	5.0
700	10.0
800	10.0
900	50.0
1000	100.0
1100	500.0

$$L_p = \sqrt{D_p \tau}$$

$$L_n = \sqrt{D_n \tau}$$

$$D_p = \frac{k_B T}{q} \mu_p$$

$$D_n = \frac{k_B T}{q} \mu_n$$

Table 1 – Absorption lengths of light through silicon based on wavelength.

14

Where D represents the diffusion coefficient, τ is the minority charge carrier lifetime and μ is the mobility of charge carriers. The carrier lifetimes are determined based upon doping concentrations in the silicon utilizing the relations [16]:

$$\tau_p = \frac{1}{(3.45 \; x \; 10^{-12})N_A + (9.5 \; x \; 10^{-32})N_A^2}$$

$$\tau_n = \frac{1}{(7.8 \; x \; 10^{-13})N_D + (1.8 \; x \; 10^{-31})N_D^2}$$

The diffusion length equations were solved in terms of doping concentrations utilizing the definitions of the diffusion coefficients and the carrier lifetimes in each region, based on assumptions of a 200 μm thick silicon substrate and a maximum voltage drop across the bulk of 50 mV. The initial 200 μm thickness was assumed to be sufficient for absorbing most of the wavelengths in the Si region (832 nm – 1148 nm) without incurring a bulk resistance that would significantly degrade V_{OC}. The resulting analysis yielded a minimum required bulk doping concentration in the p-region of $N_A = 2 \; x \; 10^{18}$ cm^{-3}. Under a doping concentration this high, Auger recombination effects greatly reduced the current collected at the Si cell electrodes, significantly degrading overall conversion efficiency in the cell. To counteract this effect, the thickness of the silicon substrate was reduced to 150 μm thick and optimized again for a maximum voltage drop of 50 mV. This yielded the final doping concentrations of $N_A = 10^{16}$ cm^{-3} in the p-region and $N_D = 2 \; x \; 10^{17}$ cm^{-3}.

The final cell configuration is shown in Figure 9, with a close-up of the CdTe top cell and electrodes shown in Figure 10.
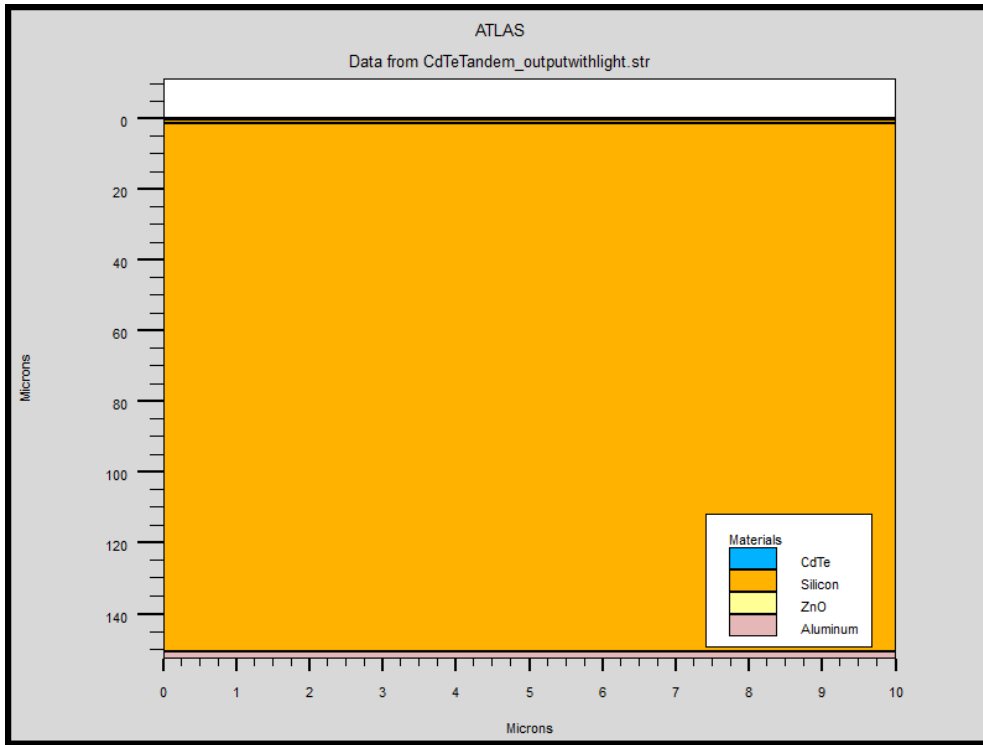
Figure 9 - Overall device structure as modelled in Atlas and plotted in TonyPlot
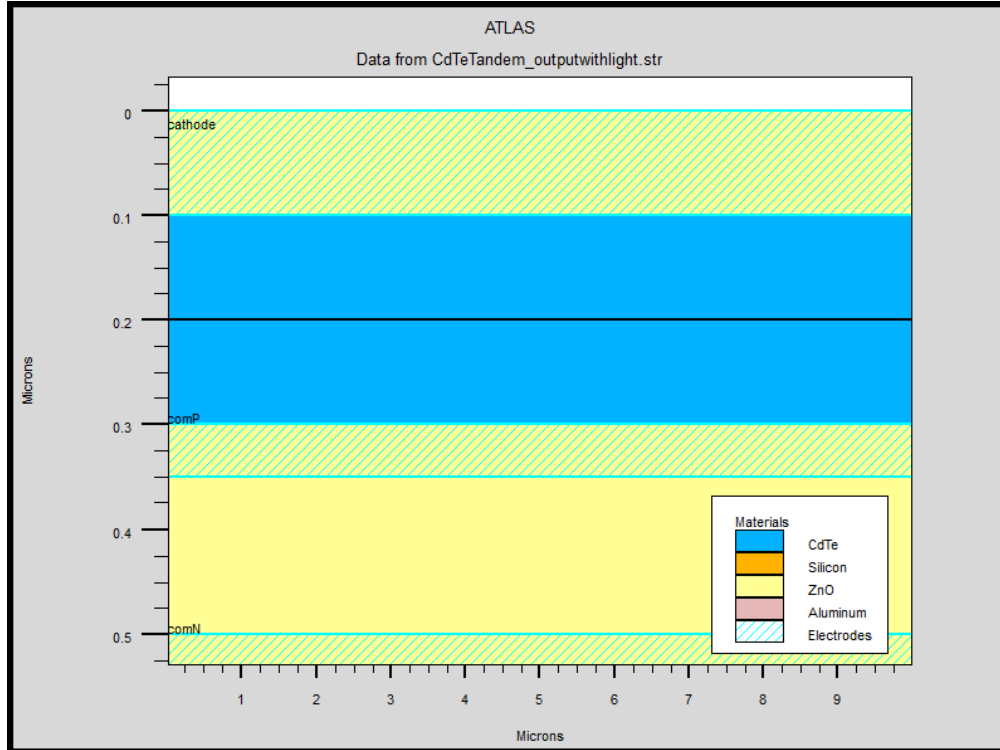

Figure 10 - Enlarged view of the CdTe layers, electrodes for the CdTe cell (cathode and comP), insulating ZnO layer between the cells and the Si cell cathode (comN), totaling only 550nm in thickness collectively
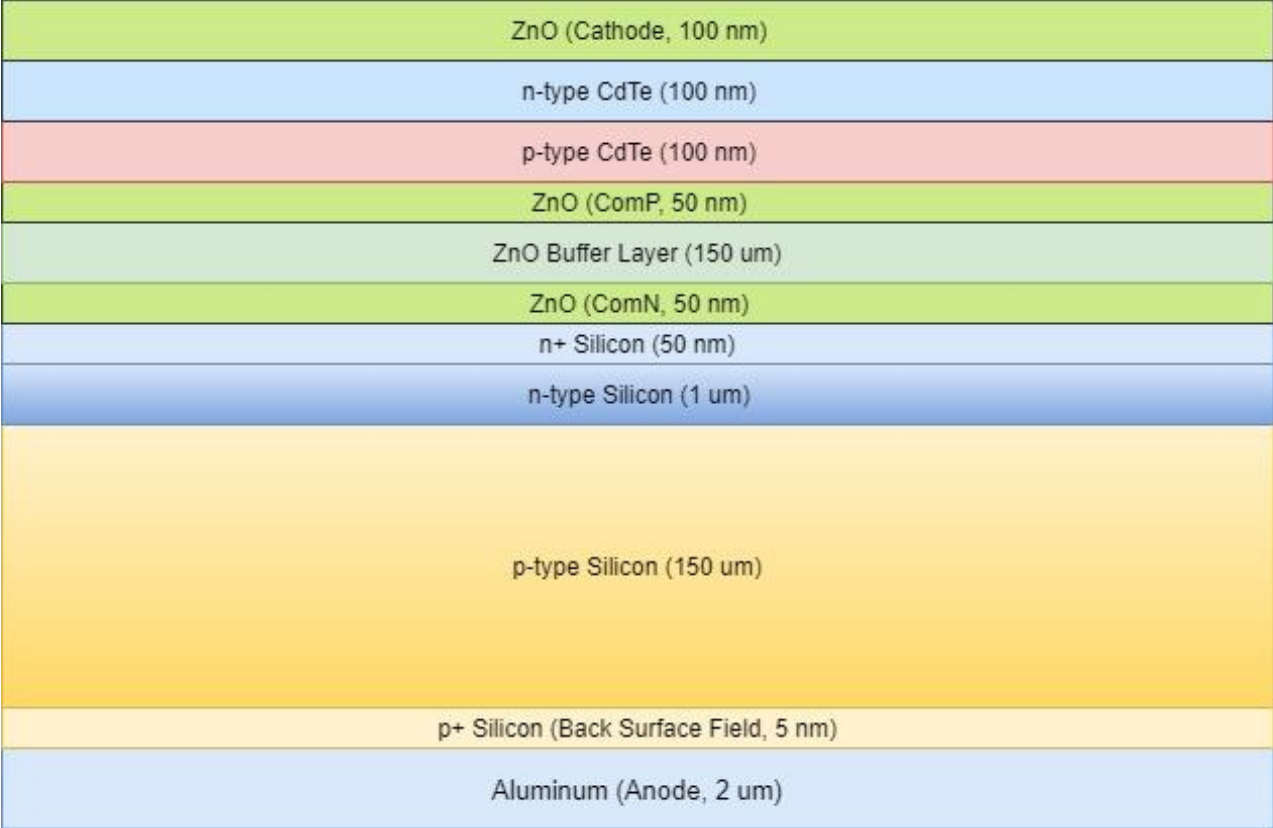
16

Figure 11 - Schematic View of CdTe/Si Tandem Cell Design (Not to Scale)

4. Results

The tandem cell, consisting of a CdTe top cell and a Si bottom cell that acts as the substrate, was modelled with four electrodes:

1. Cathode – acts as the cathode for the CdTe cell

2. ComP – acts as the anode for the CdTe cell and the point of reference for the analysis of the top cell's electrical characteristics

3. ComN – acts as the cathode for the Si cell

4. Anode – acts as the anode for the Si cell and the point of reference for the analysis of the bottom cell's electrical characteristics

The ComP and ComN electrodes are separated by an undoped layer of ZnO, which acts as a transparent electrical insulator. It would require a more elaborate inverter to connect a four-terminal tandem cell to a grid than what would be required for a more traditional three-terminal device, but the electrical separation of the subcells allows them to be optimized separately without the need to match current outputs, which could limit the overall cell conversion efficiency. The dimensions of the cell in the simulation are 10 microns wide and 152.6 microns deep, with a default thickness of 1 micron. The ambient temperature assumed is 300K ($27^{\circ C}$).

Material	Bandgap (eV)	Carrier Lifetime (ns)	Intrinsic Carrier Concentration (cm^{-3})	Dopant Concentration (cm^{-3})	Carrier Mobility (cm^2/Vs)
CdTe	1.48	333	1×10^6	1×10^{15}	Und. in material models
n-type Silicon	1.09	12,531	1×10^{10}	1×10^{17}	781
p-type Silicon	1.09	28,977	1×10^{10}	1×10^{16}	437

Table 2 - Material properties of semiconductor materials used in the simulation

Figure 12 shows the I-V characteristics of the CdTe top cell when illuminated under an AM1.5 spectrum at a 90° incident angle (perpendicular to the plane of the cell surface), which is the point at which the most light is able to be absorbed by the cell. The I-V curve was generated by varying the applied voltage at the CdTe cell anode (ComP) while under illumination and measuring the resulting current, which encompasses both drift current density (J_{drift}) and diffusion current density (J_{diff}).
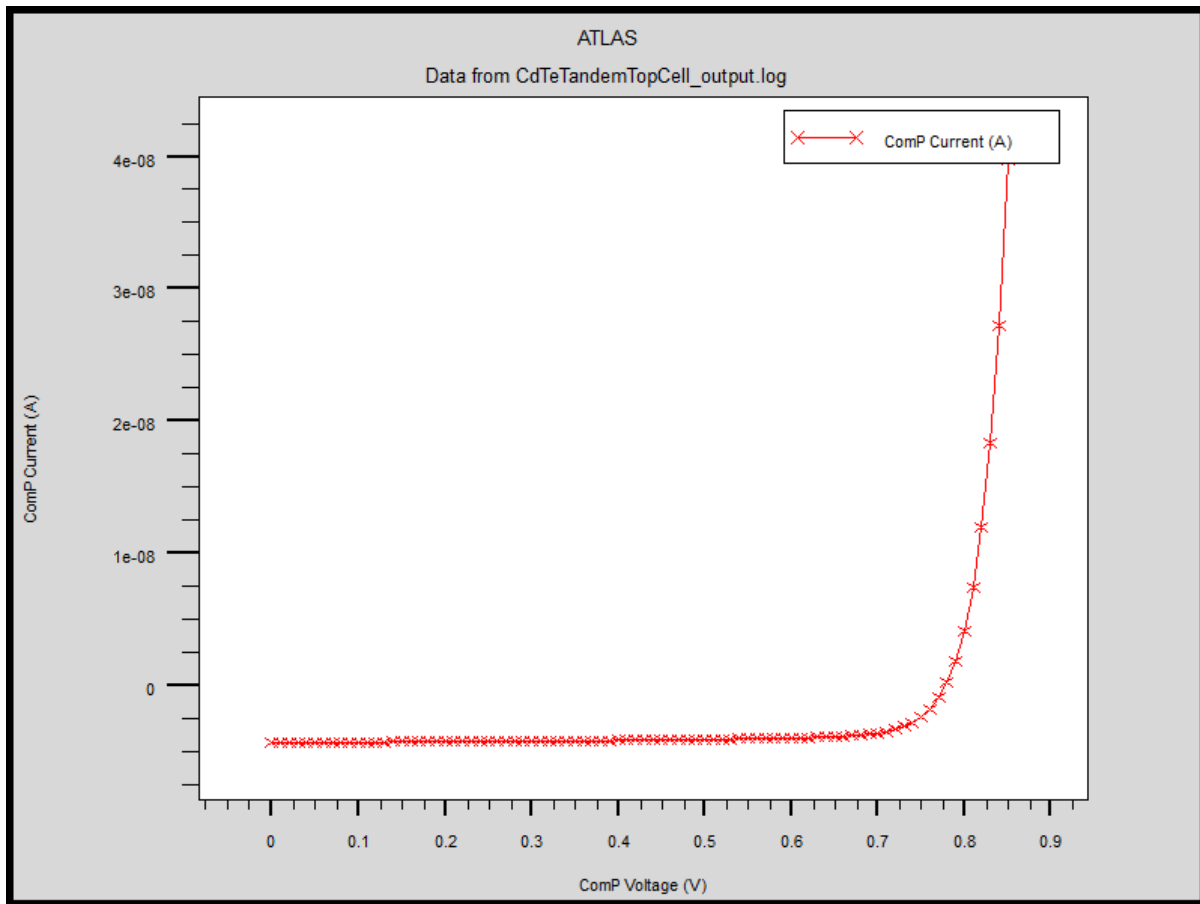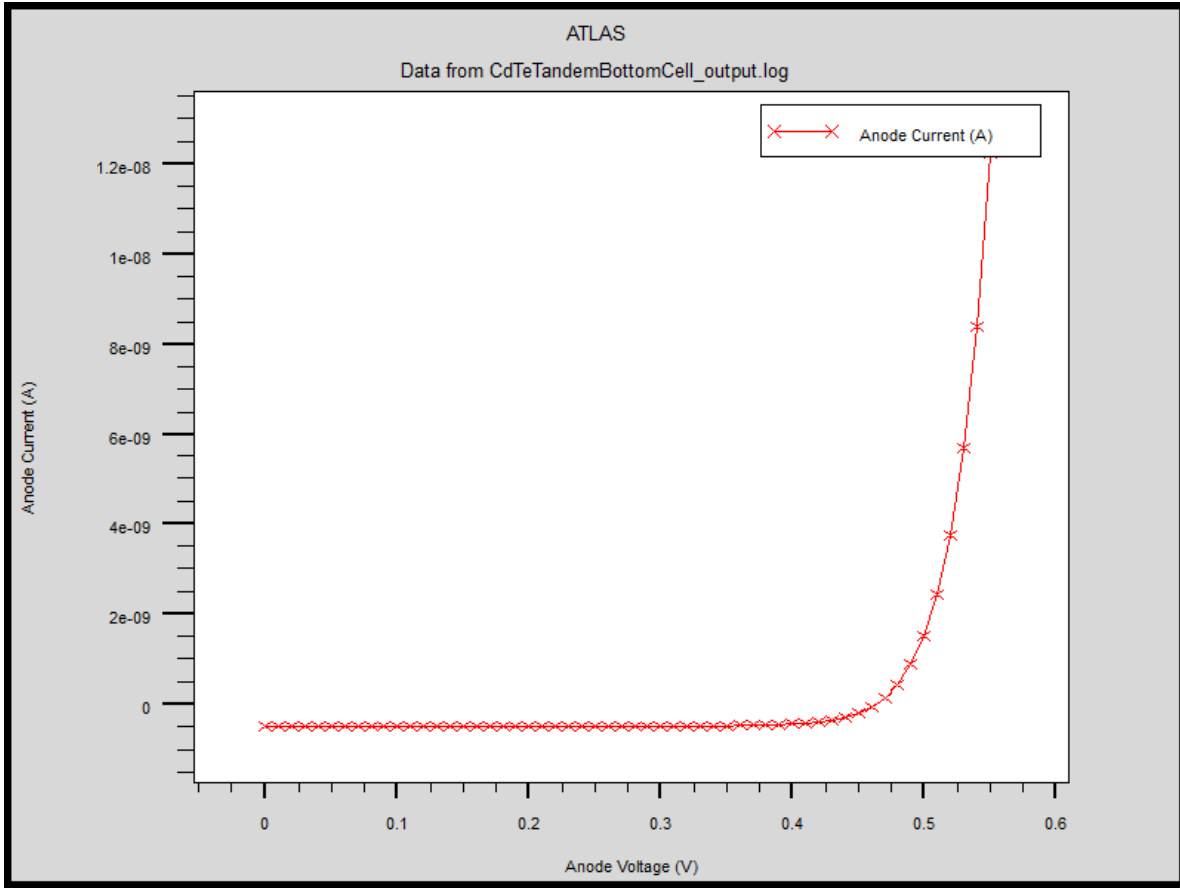

Figure 12 - CdTe Top Cell I-V Curve, evaluated using the electrode ComP as the reference

The current measured when the applied voltage is 0V is the short-circuit current (I_{SC}). The voltage applied that biases the p-n junction to act as a forward-biased diode and prevent any current flow to the anode is the open-circuit voltage (V_{OC}) [16]. The shape of the curve, with an

incredibly long and flat current profile over a large span of voltages, is indicative of a cell with a favorable fill factor (FF), which bodes well for the overall conversion efficiency. The equation for calculating fill factor is located in the "Methods and Design" section. V_{OC} and I_{SC} can be approximated using a visual inspection of the I-V curve, but were extracted in a subsequent simulation step and will be explored in greater detail later.

Figure 13 shows the I-V characteristics of the Si bottom cell when illuminated under an AM1.5 spectrum at a 90° incident angle (perpendicular to the plane of the cell surface), which is the point at which the most light is able to be absorbed by the cell. It is important to recall that the Si cell receives a significantly lower intensity of radiation than the CdTe cell does due to the effects of light absorption in the CdTe layers and the reflection of a small percentage of light (10%-15%) off the ZnO layers. This leads to an overall lower current density due to a lowered photogeneration rate, which will be explored in more detail later.

Figure 14 – Si Bottom Cell I-V Curve, evaluated using the electrode Anode as the reference

The Si cell I-V curve reveals that the Si cell has significantly lower V_{OC} and I_{SC} than the CdTe cell, which indicates that it will contribute less to the overall conversion efficiency of the tandem cell, which confirms predictions made based upon the optical intensity and photocurrent profiles of Figures 7 & 8. However, the rectangular profile of the Si I-V curve indicates that it should benefit from having a higher fill factor than the CdTe cell, which will improve the conversion efficiency of the Si cell. This can be attributed to the higher doping concentrations in the silicon regions, which reduce the series resistance of the semiconductors [17].

A closer look at the physical phenomena in the CdTe top cell reveals why the I_{SC} and V_{OC} of the CdTe cell are so high. Figure 15 shows the charge concentration in the CdTe absorbers.

The charges are evenly distributed on either side of the p-n junction at a concentration of approximately 150 μC/cm^3. The charge concentration profile is evidence that the depletion region in the CdTe absorbers spans nearly the entirety of the CdTe layers, which allows for high charge carrier collection efficiency by the electrodes and a low recombination rate.
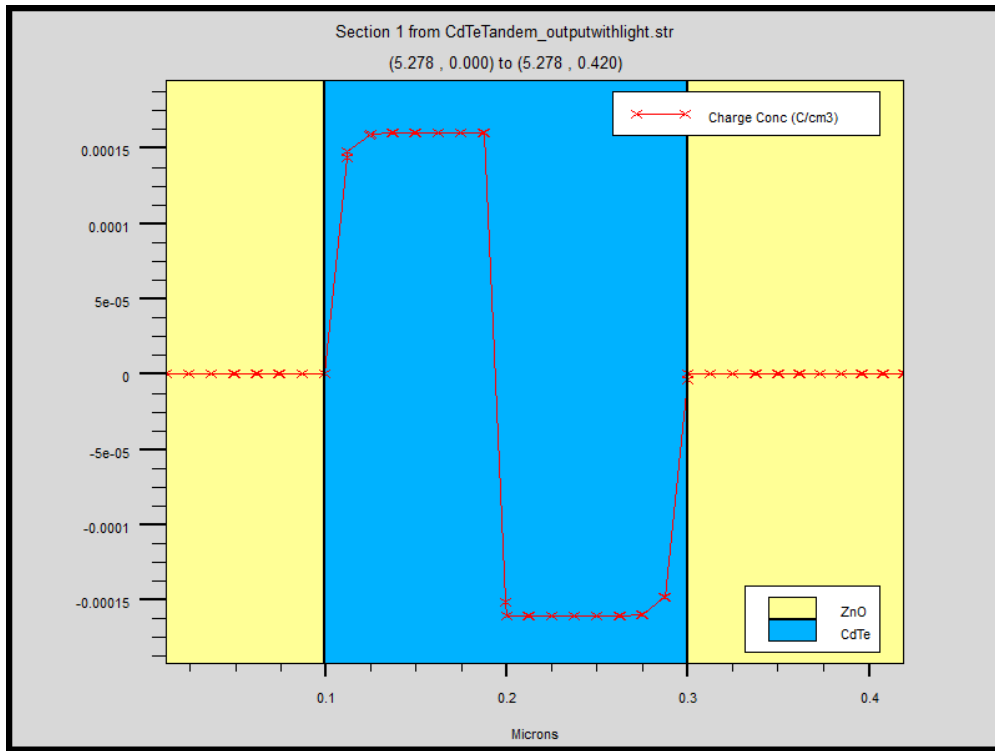
Figure 15 - Charge concentration in the CdTe absorber layers

Figure 16, showing the electric field profile in the CdTe absorbers and the electrodes adjacent to them, further supports the conclusion that the depletion region spans the entirety of the CdTe layers.
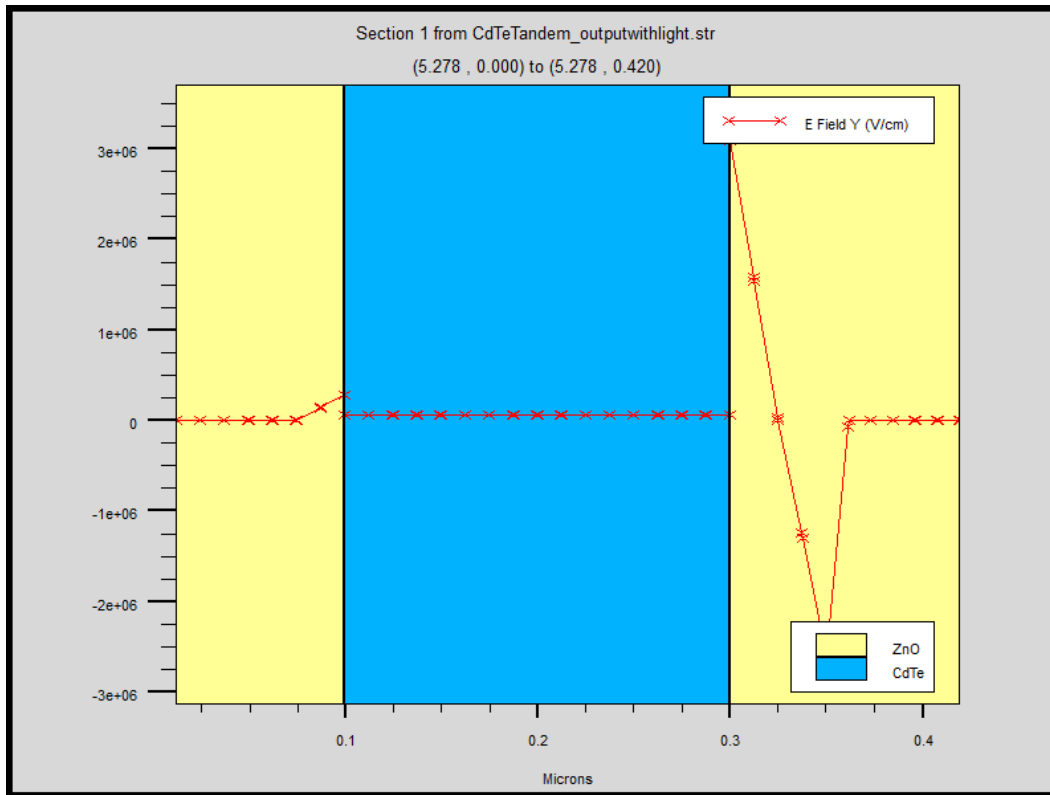
Figure 16 - Electric field profile in the CdTe Top Cell absorber layers and electrodes

The positive electric field in the depletion region, with a magnitude of approximately 20,000 V/cm, will act as an electromotive force to help "sweep" the current towards the cathode [16]. When the charge carriers recombine at the interface with the ZnO electrodes, it creates a high magnitude positive electric field. The separate electron and hole current densities can be seen in Figure 17 below.
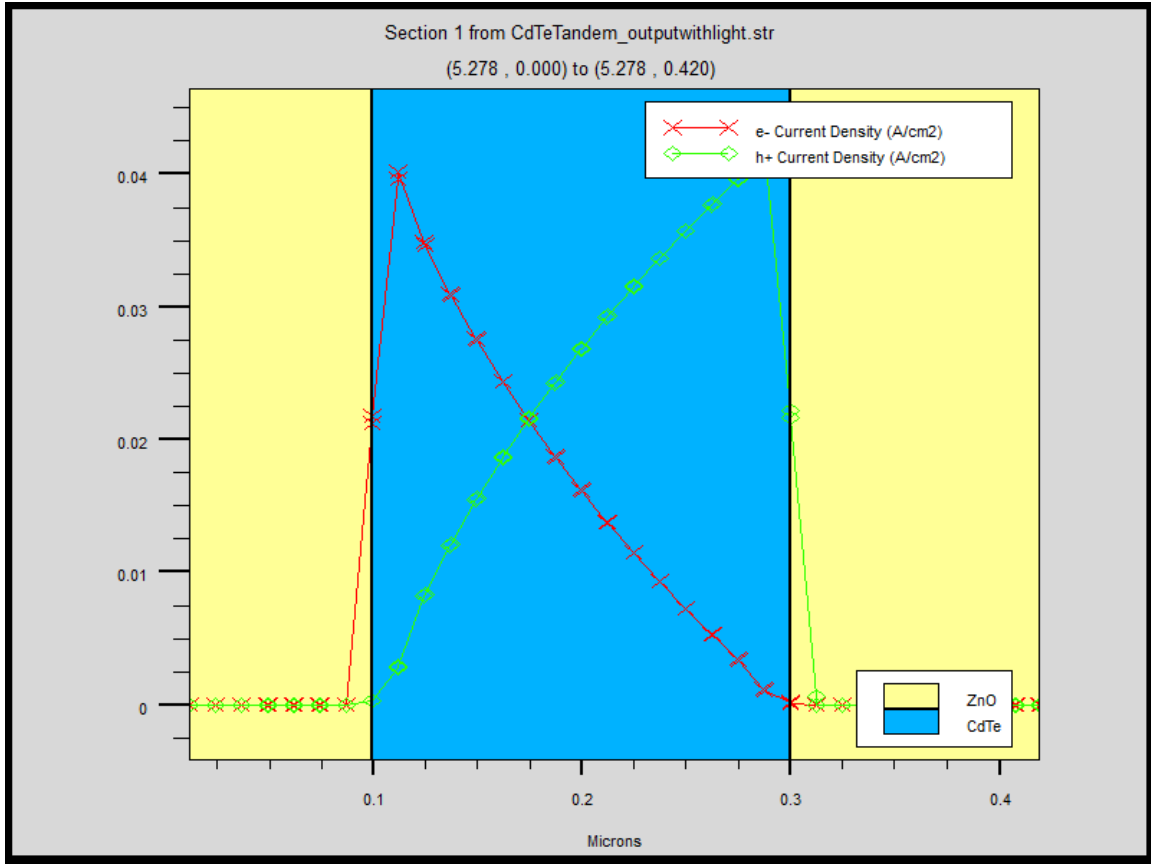
Figure 17 - Electron and hole current densities in the CdTe absorber layers

The electron and hole currents are well segregated from one another by the time the charge carriers reach the electrodes. This is a direct result of the sweeping effect of the positive electric field and the dopant atoms being evenly distributed in the n-region and the p-region. The hole current has a slightly higher peak density than the electron current, which can be explained by looking at the charge carrier recombination rate profile for the CdTe top cell in Figure 17.
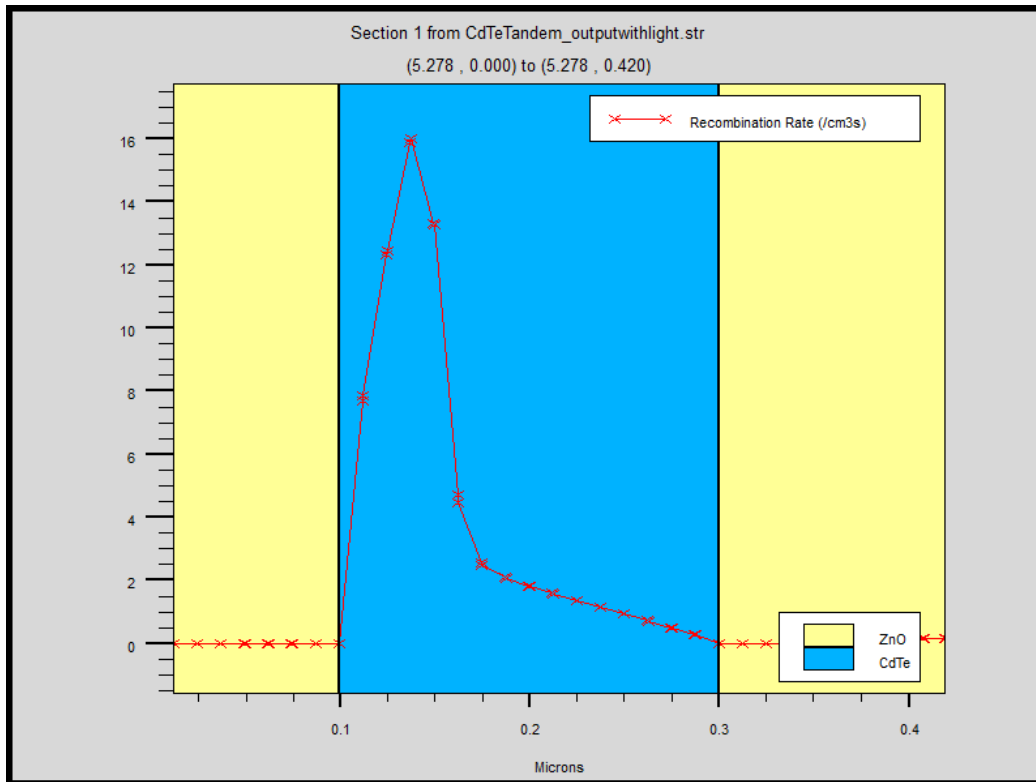
Figure 18 - Recombination rate of charge carriers in the CdTe absorbers

The charge carrier recombination rate, which peaks at an incredibly low value of approximately 16 $cm^{-3}s$, is higher in the n-CdTe region than it is in the p-CdTe region. This can be attributed to the incredibly high carrier mobility in the n-region at such a low doping concentration ($N_D = 10^{15}$ cm^{-3}) causing electrons and holes to make contact with one another and recombine, in spite of the relatively long charge carrier lifetimes and presence of the depletion region throughout the n-region.

In order to understand the effect that the CdTe cell has on the optical intensity of the radiation that eventually reaches the Si bottom cell, the photogeneration rate profile (Figure 19) and optical intensity profile (Figure 20) of the CdTe cell must be analyzed.
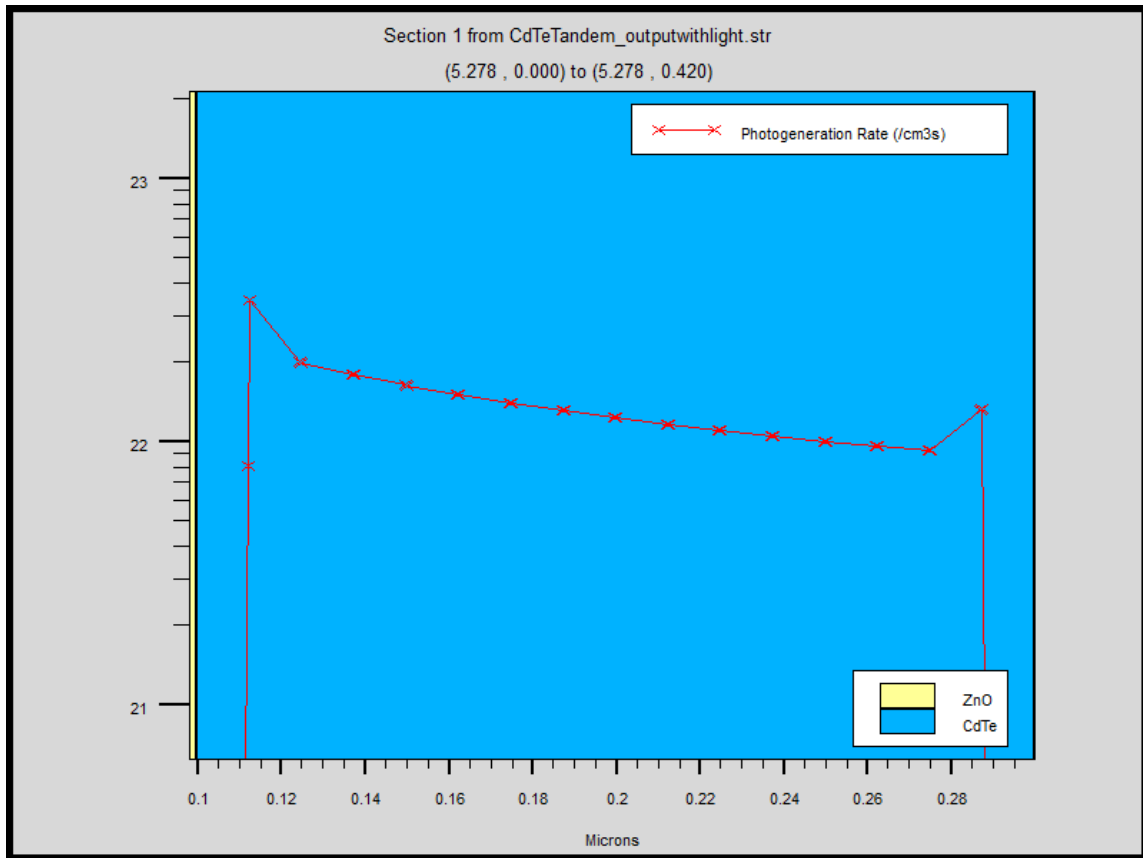
Figure 19 - Photogeneration rate in the CdTe Top Cell

The photogeneration rate through the CdTe absorber layers gradually drops from a peak of approximately 4 x 10^{22} cm^{-3}s to approximately 2 x 10^{22} cm^{-3}s, a decrease of about 50%. This profile is in line with the optical intensity trend in Figure 20.
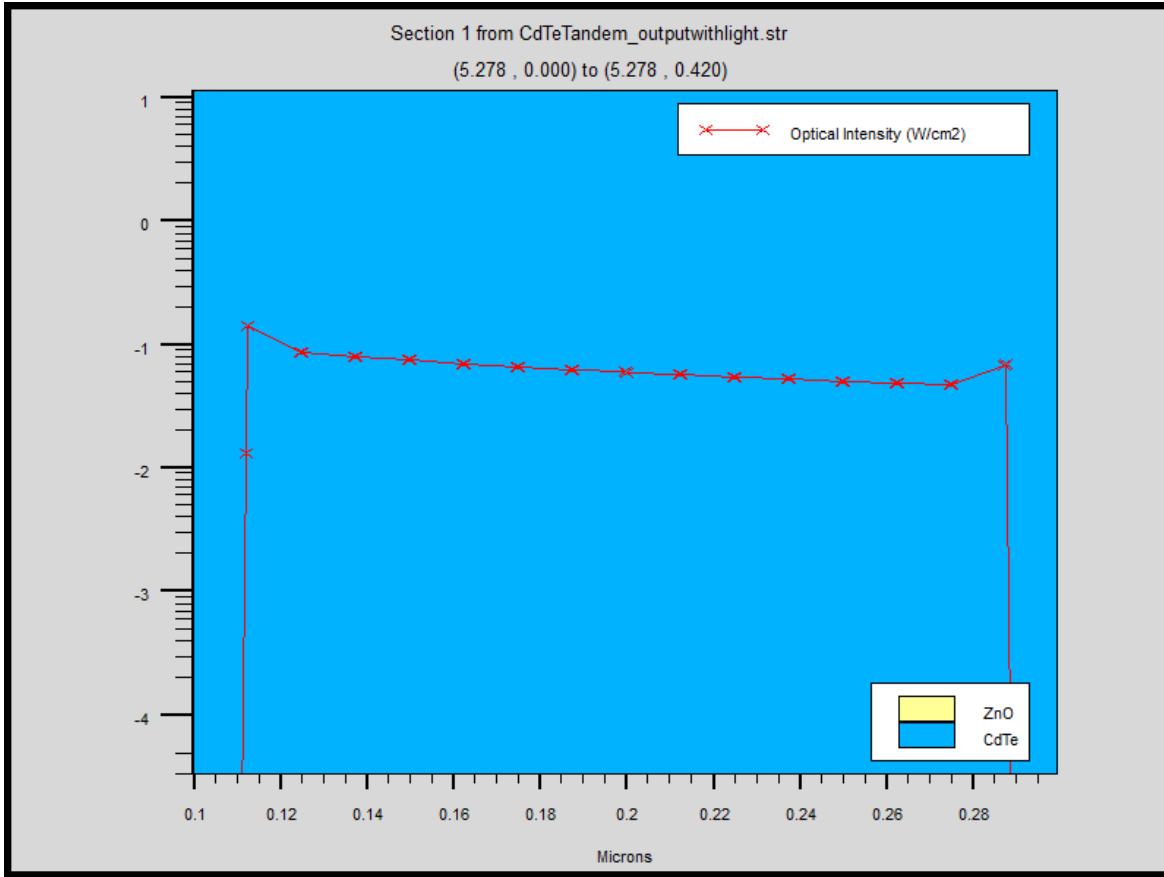
Figure 20 - Optical intensity through the CdTe absorber layers

The optical intensity peaks on the surface of the cell at approximately 0.1 W/cm^2 (1000 W/m^2), the standard incident intensity for the AM1.5 spectrum, and tapers off to approximately 0.06 W/cm^2 (600 W/m^2) as photons are absorbed in the CdTe layers to create exciton pairs. The absorption of light in the CdTe layer greatly reduces the amount of light that reaches the surface of the Si cell, but the high photovoltaic action in the CdTe cell yields a promisingly efficient energy conversion.

When the operating parameters are extracted, the yield is I_{SC} = -4.29864 x 10^{-9} A, V_{OC} = 0.778623 V, P_{max} = -2.53892 x 10^{-9} W, FF = 0.758912 and a conversion efficiency of η = 25.3892% for the CdTe cell alone. When these results are extrapolated over the size of a standard industrial solar cell (39 in. x 77 in.), the CdTe cell contributes 492 W nominal per cell.

27

The Si cell analysis begins by observing the doping profiles in the Si cell, which are modelled after the standard Si cell architecture shown in Figure 4.
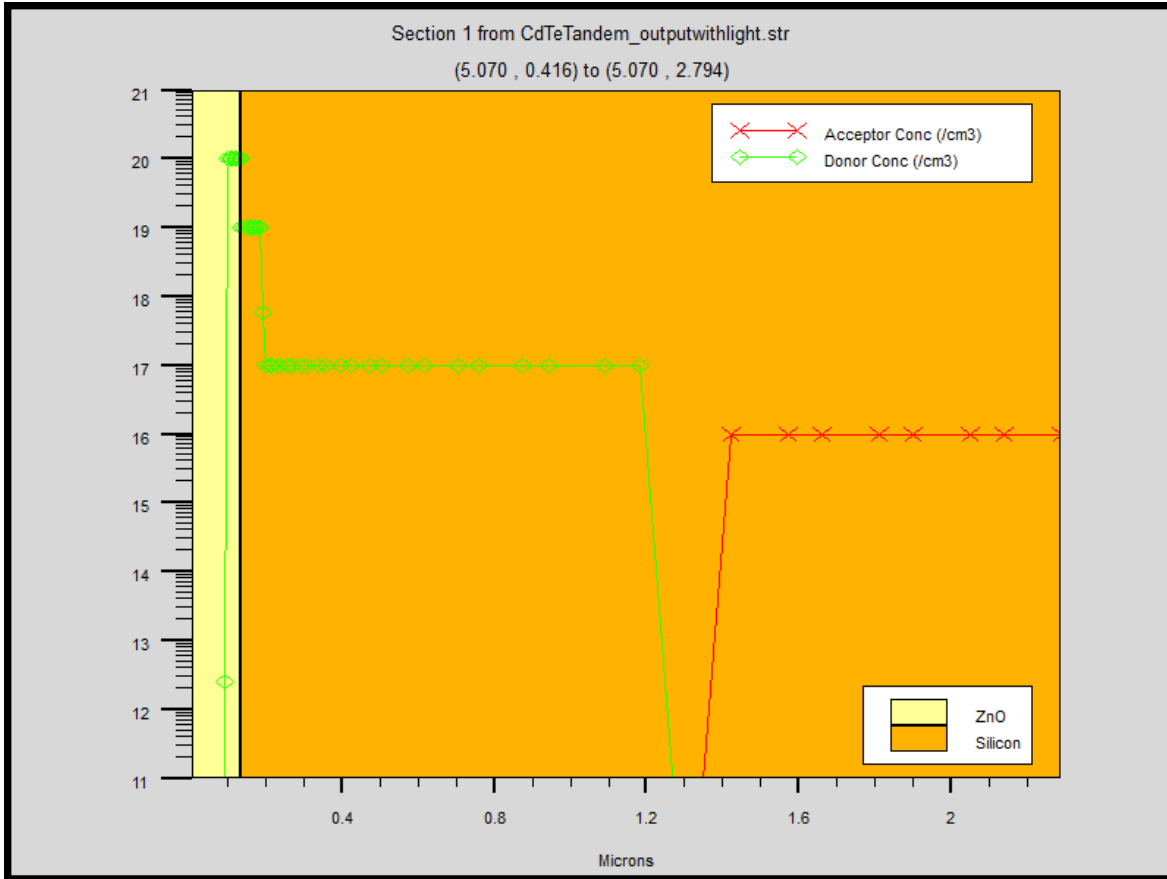
Figure 21 - Acceptor and Donor Atom concentrations in the Si absorber layers

The first 50 nm of the Si n-region absorber is heavily doped at $N_D = 10^{19}$ cm^{-3} in order to form a good ohmic contact with the ZnO cathode (ComN) [17]. This forms a sort of recombination layer immediately adjacent to the cathode for more effective current injection. The next 1 μm of silicon depth is uniformly doped at $N_D = 10^{17}$ cm^{-3} to form the n-region absorber of the Si cell. From there, the p-region of the cell is doped uniformly at $N_A = 10^{16}$ cm^{-3}, which is low enough to combat the effects of recombination through the bulk of the silicon without having a significant adverse impact on the series resistance of the cell. Though not visible in Figure 21, there is also a heavily doped, 5 nm thick p-region adjacent to the interface

between the silicon and the aluminum back contact to form a Back Surface Field (BSF) for good ohmic contact and charge carrier recombination at that interface.

The charge concentration profile for the Si cell at the interface between the n+ and n regions is shown in Figure 22. Even though both are doped with donor atoms, the 100x difference in magnitude creates a shallow p-n junction between the two regions, resulting in a positive electric field that "sweeps" holes towards the cathode.
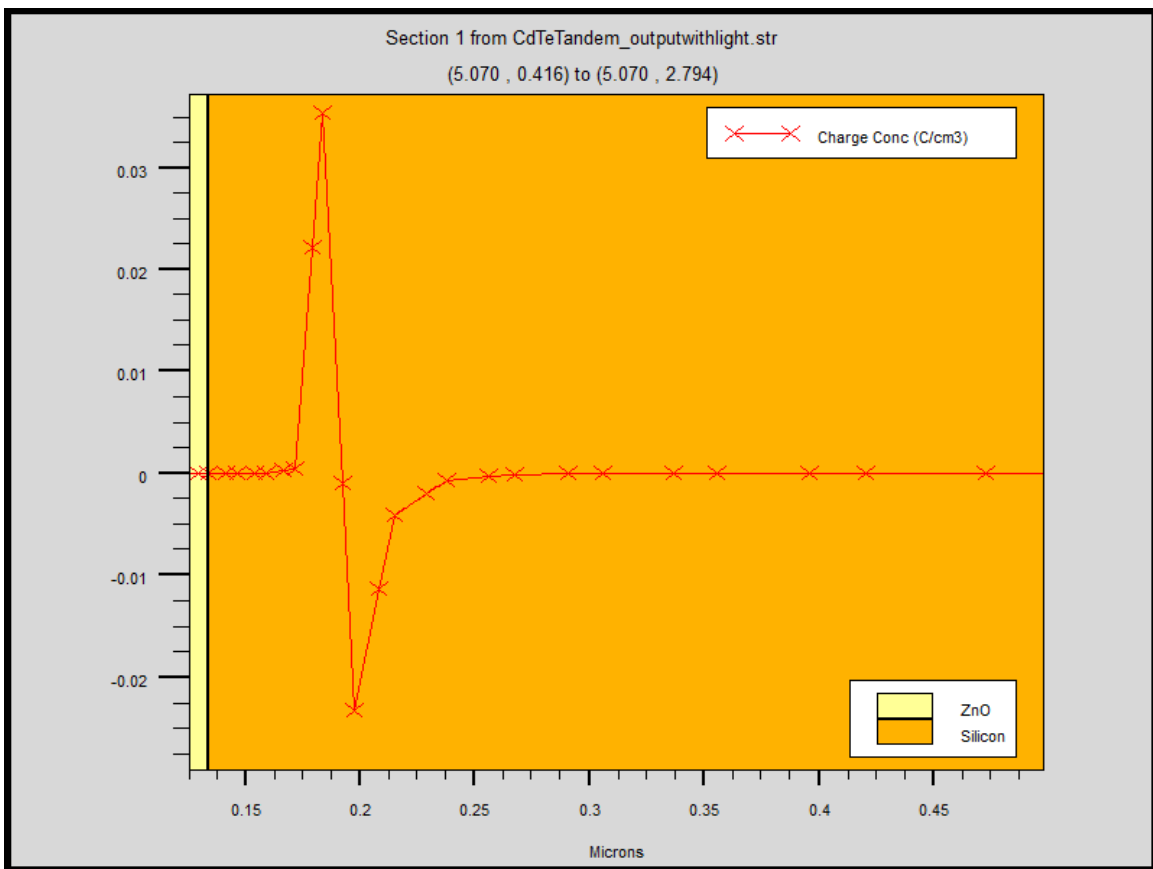
Figure 22 - Charge concentration at the interface between the n and n+ regions of the Si cell

The charge profile at the Si p-n junction, shown in Figure 23, shows a far smoother gradient in the charge concentration. The peak concentration in both the positive and negative regions is approximately 0.002 C/cm^3, which is higher than the peak concentration in the CdTe

absorber layers (0.00015 C/cm^3). Despite the lower optical intensity of light that reaches this junction, the higher doping concentrations in the silicon as compared to the CdTe provide a greater density of possible exciton pairs. The width of the non-zero charge concentration regions also corresponds to the width of the depletion region [16], which is approximately 700 nm.
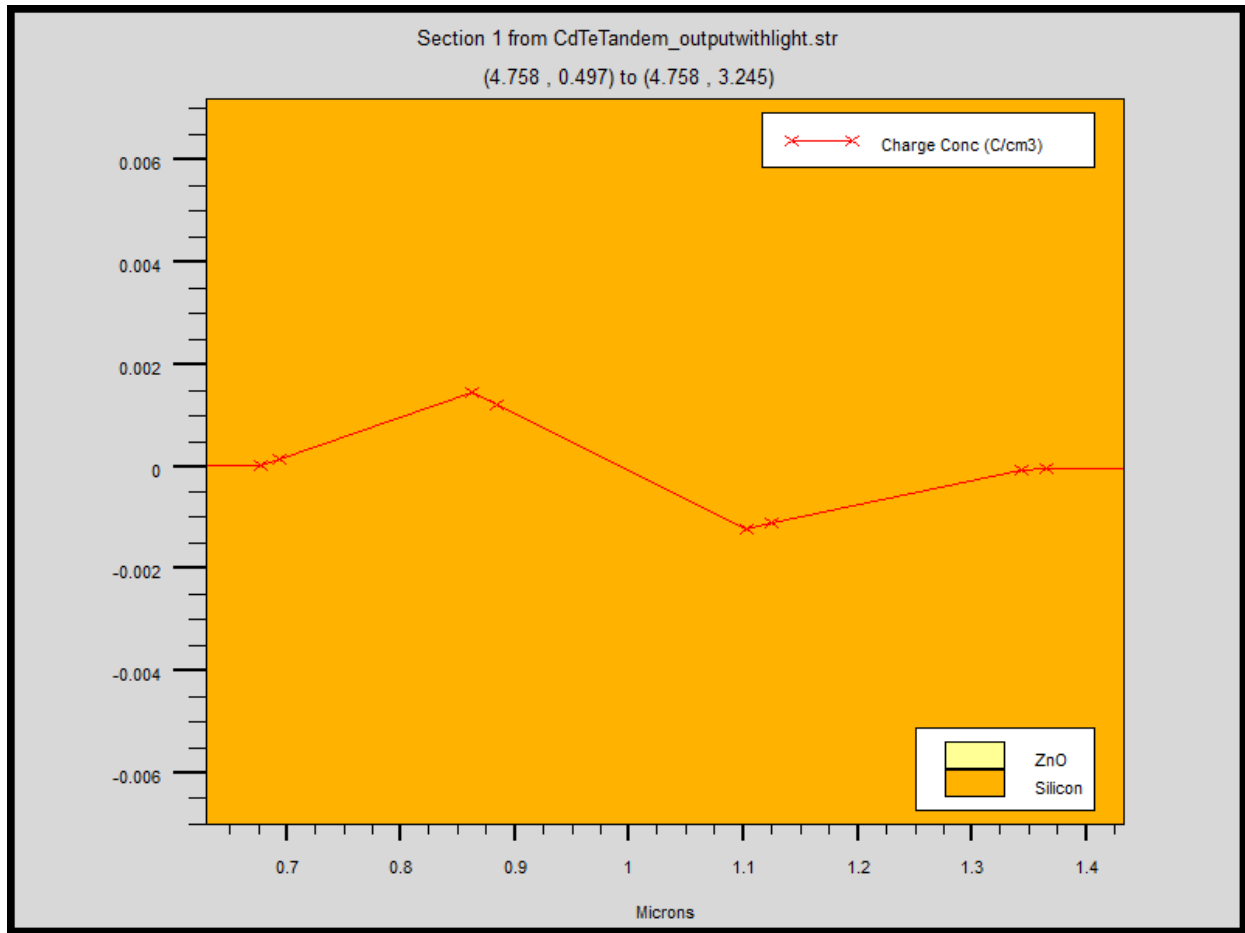
Figure 23 - Charge concentration at the Si p-n junction

The electric field profile at the silicon p-n junction in Figure 24 is similar in nature to that seen in the CdTe cell (Figure 15).
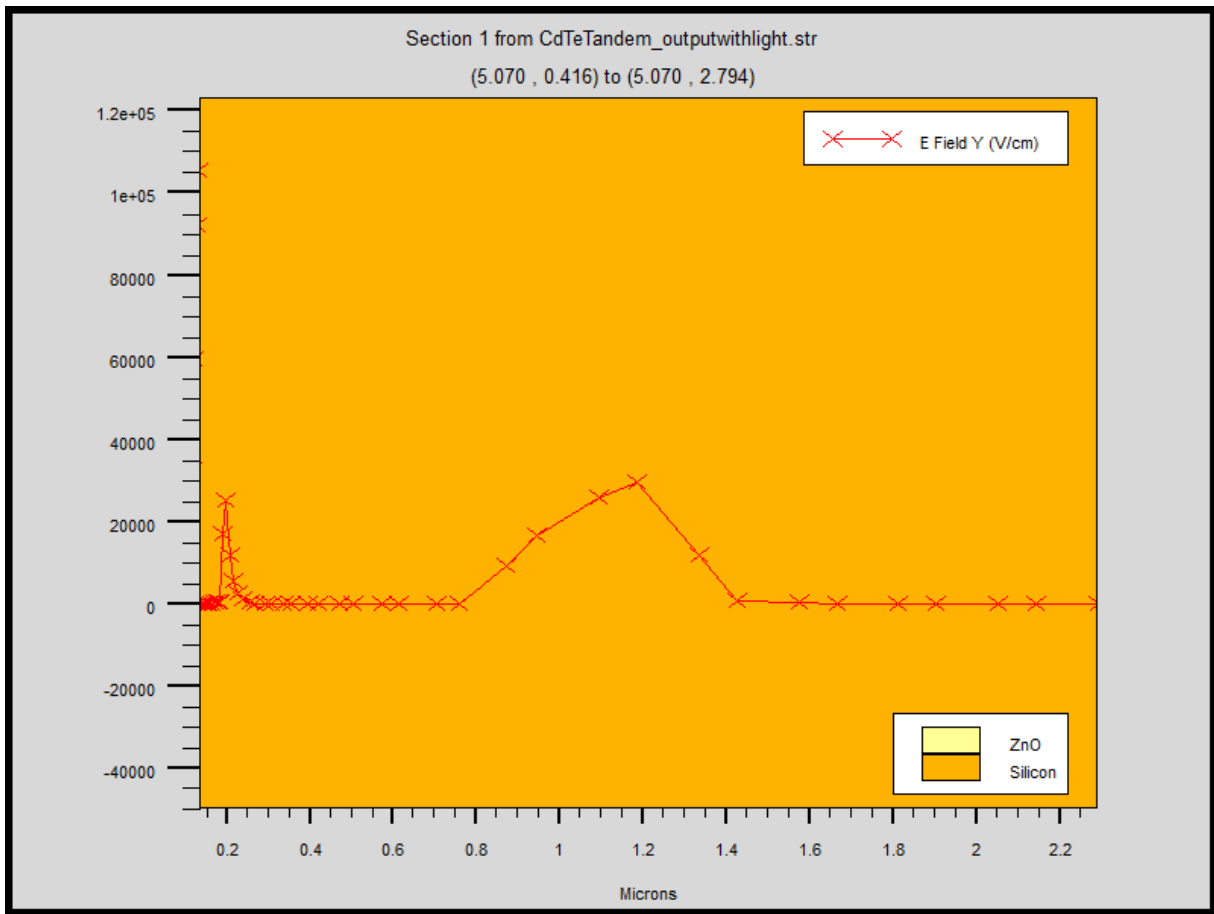
Figure 24 - Electric field profile of the Si bottom cell

At both the n+-n junction and the p-n junction, there is a high magnitude positive electric field to assist in "separating" electron and hole currents and move them towards the correct electrode. In the instance of the p-n junction, the electric field magnitude is approximately 30,000 V/cm, as compared to a magnitude of 20,000 V/cm at the CdTe p-n junction. This is due in large part to the higher dopant concentrations in the silicon. It is also necessary for the electric field to be greater in order to combat the recombination losses through the bulk of the Si cell, which is many times thicker than the CdTe layer.

The electron and hole current density profiles for the Si cell are shown in Figure 25.
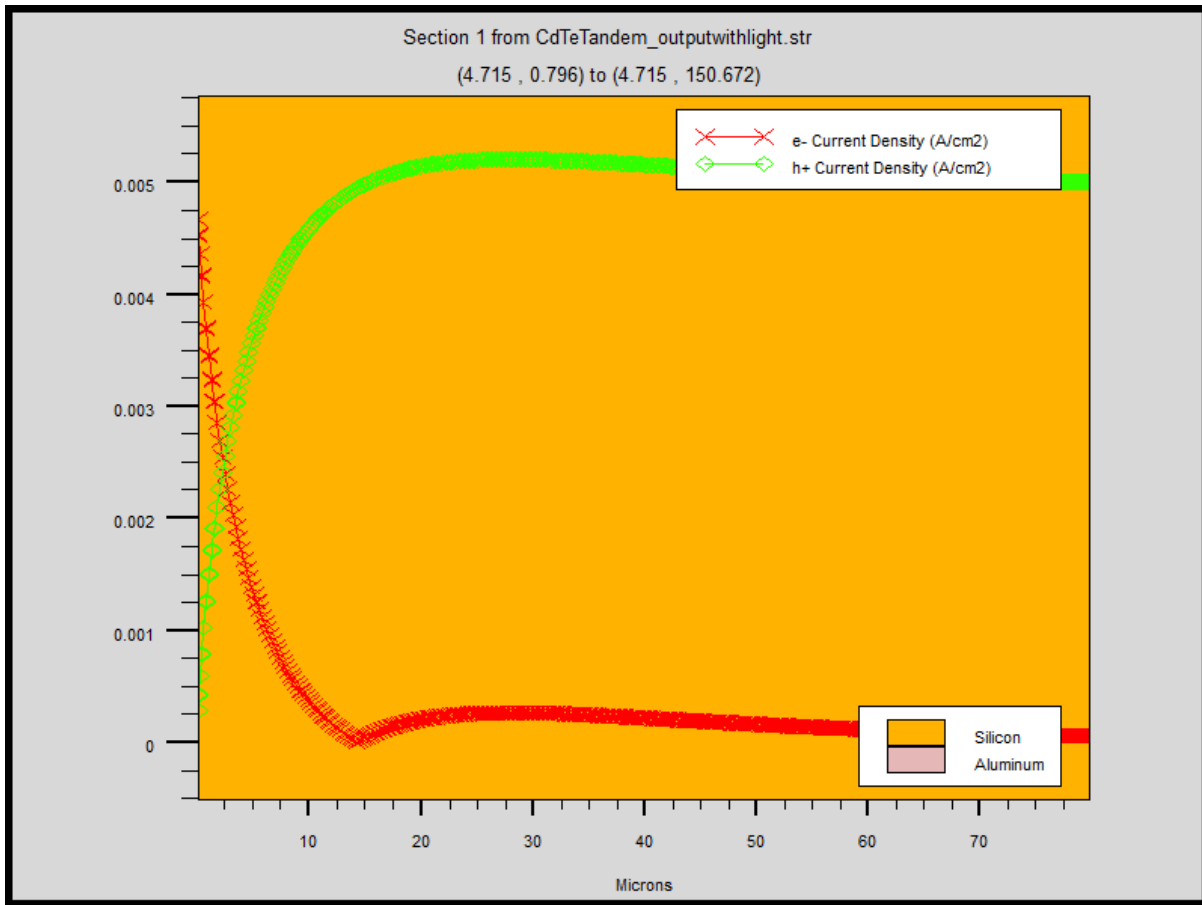
Figure 25 - Electron and Hole current densities in the Si bottom cell

The crossing point of the electron and hole current densities corresponds to the depth where the magnitude of the electric field peaks. Due to the thickness of the silicon substrate, which is necessary for achieving the minimum absorption lengths of the radiation wavelengths available to the silicon absorbers, there is a tapering off of hole current density as it moves through the silicon. The peak magnitude of the current densities, at 0.005 A/cm^2, is significantly lower than the current density seen in the CdTe absorber layers at 0.04 A/cm^2. This is caused by the lower optical intensity and higher recombination rates in the silicon.

The optical intensity profile through the Si cell is shown in Figure 26.
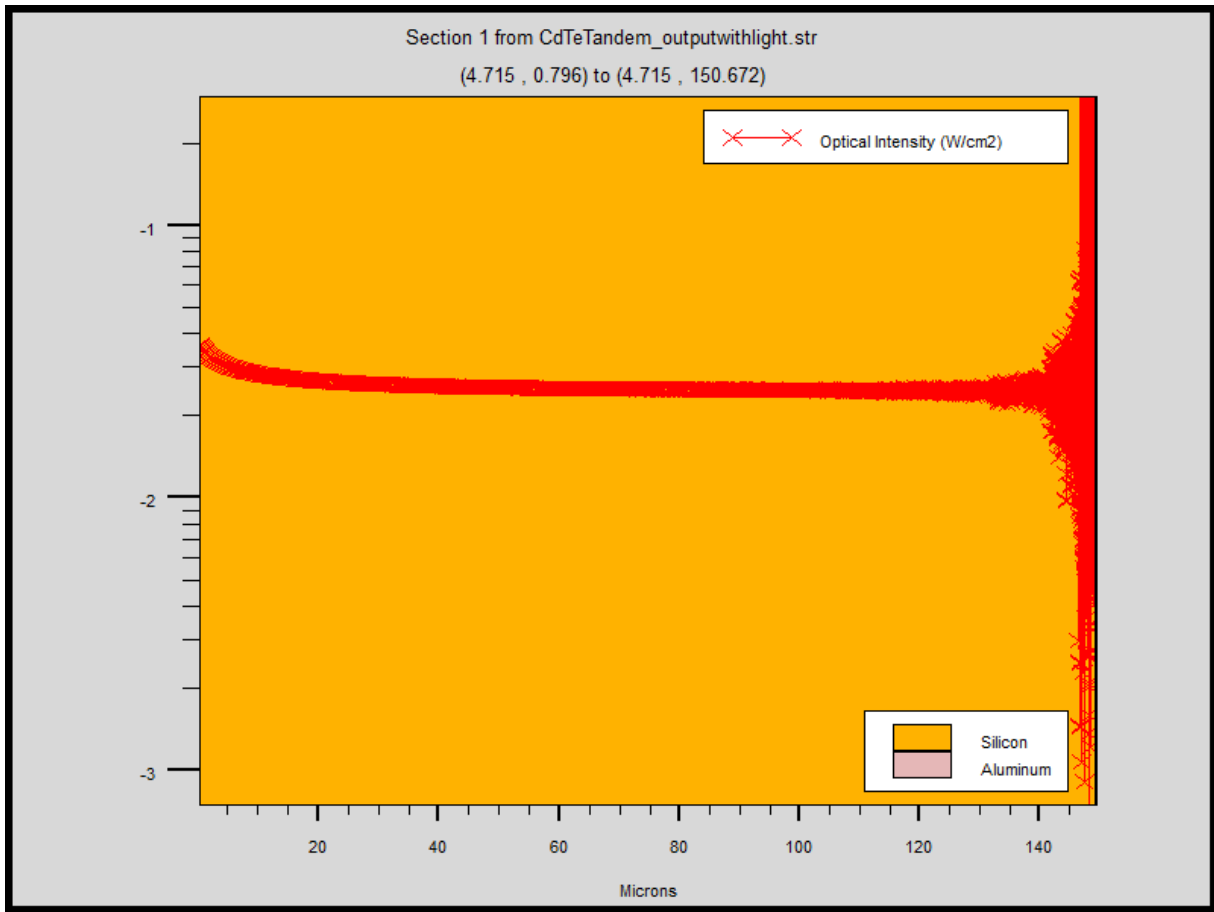
Figure 26 - Optical intensity profile through the Si bottom cell

The optical intensity that reaches the surface of the silicon is approximately 0.04 W/cm^2 (400 W/m^2), which is 40% of the radiation intensity available at the surface of the CdTe. This is the primary driver for the lower current densities and the need for higher doping concentrations in the silicon than in the CdTe. It is also worth noting that about 0.025 W/cm^2 (250 W/m^2) reaches the back surface of the cell, meaning that approximately 25% of incident light is not absorbed by the cells. This radiation consists of all the wavelengths in the AM1.5 spectrum above the 1148 nm wavelength that can be absorbed by silicon with a bandgap energy of 1.09 eV. The seeming aberrations in the profile near the Si-aluminum interface are caused by the reflection of light off the aluminum, which actually contributes to improving photogeneration rate in the cell by

increasing the effective path length of the photons through the silicon, allowing more photons to be absorbed.

Figure 27 overlays the photogeneration rate and the recombination rate for the Si bottom cell. It is important to note that the left vertical axis is the scale for the recombination rate and the right vertical axis is the scale for the photogeneration rate.
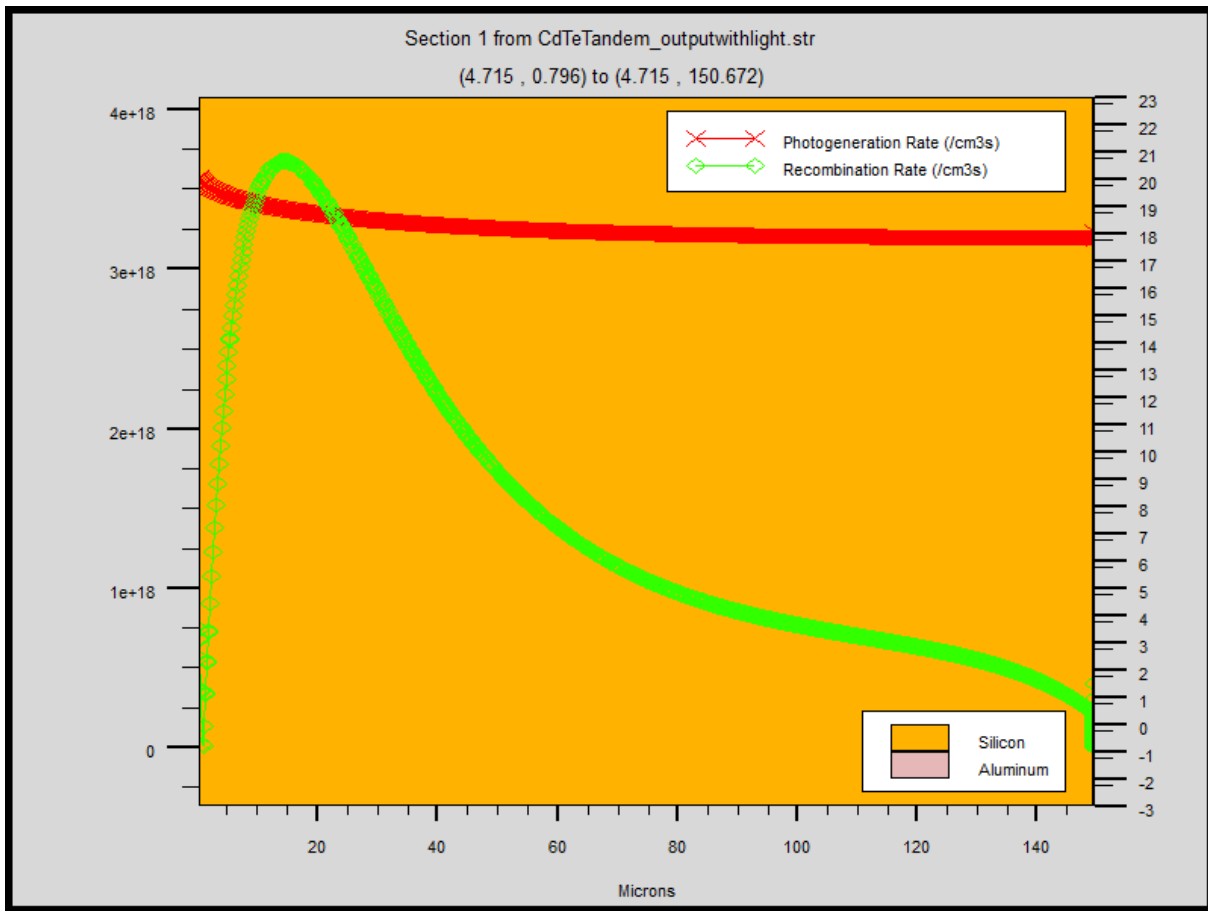
Figure 27 - Photogeneration Rate and Recombination Rate for the Si bottom cell

The photogeneration rate follows the optical intensity profile, with a peak value of approximately 10^{20} cm^{-3}s and a lower value of approximately 10^{18} cm^{-3}s. These are both significantly lower than the rates in the CdTe absorbers (2×10^{23} to 4×10^{23} cm^{-3}s), due to the lower optical intensity and longer absorption lengths of the available radiation wavelengths in the silicon. The

recombination rate is also very high, approximately 3.8 x 10^{18} cm^{-3}s, once the charge carriers have been swept more than one diffusion length away from the end of the p-n junction depletion region. The recombination in the silicon bulk is primarily Shockley-Read-Hall recombination, in which an electron falls into a "trap" state, an energy level within the bandgap created by a defect [16]. There are also some Auger recombination effects in the heavily doped n+ and p+ regions at the Si-electrode interfaces, which is caused when an electron and hole recombine in a band-to-band transition in a heavily doped semiconductor [13].

When the operating parameters are extracted, the yield is I_{SC} = -4.94757 x 10^{-10} A, V_{OC} = 0.463052 V, P_{max} = -1.80758 x 10^{-10} W, FF = 0.788998 and a conversion efficiency of η = 1.80758% for the Si cell alone. When these results are extrapolated over the size of a standard industrial solar cell (39 in. x 77 in.), the Si cell contributes 35 W nominal per cell.

Combining the effects of both the CdTe cell and the Si cell, the simulation yields that the tandem cell is capable of producing 527 W nominal at a conversion efficiency of η = 27.19678% under AM1.5 radiation.

Table 3 summarizes the operating parameters of each sub-cell as the incident angle of the radiation is varied from θ = 15° to θ = 90° in increments of 15°, simulating the path of the sun from sunrise to its zenith.

Inc. Angle (θ)	CdTe Cell Operating Parameters					Si Cell Operating Parameters					
	I_{SC} (A)	V_{OC} (V)	P_{max} (W)	FF	η (%)	I_{SC} (A)	V_{OC} (V)	P_{max} (W)	FF	η (%)	$\eta_{combined}$
90	8326.5	.778263	4917.9	.758912	25.3892	958.3	.463052	350.1	.788998	1.80758	27.19678
75	6450.5	.771239	3786.7	.761163	19.5492	819.5	.459318	296.2	.787048	1.52936	21.07856
60	5208.1	.765192	3047.7	.764752	15.7342	657.7	.453299	234.3	.785973	1.20978	16.94398
45	3854.2	.757013	2240.4	.767888	11.5665	492.7	.445809	171.9	.782745	.887459	12.45405
30	2467.8	.744626	1416.1	.770647	7.31088	319.8	.434603	108.3	.779332	.559136	7.870016
15	1148.4	.723559	643.1	.773884	3.31989	150.4	.415087	48.2	.772939	.249079	3.568969

Table 3 - Cell operating parameters at different radiation incident angles – note that current and power are normalized to the size of standard industrial solar cell, 39 in x 77 in.

As the incident angle decreases towards the horizontal (parallel with the plane of the tandem cell surface), the mean path length of the photons as they travel through the cells decreases, reducing the number of exciton pairs created and the photocurrent generated. This is consistent with results seen for virtually any photovoltaic cell and can be combatted in practice through the use of a pivoting stand for the solar cells that is directed by a tracking algorithm to "follow" the path of the sun and maximize the incident angle.

5. **Economic Analysis**

The viability of the production and application of a solar cell on an industrial scale is driven by its cost per peak Watt generated [1]. The current cost of a polycrystalline solar cell module at $\eta = 18.7\%$ and a 160 micron substrate thickness is approximately \$0.81 per Watt peak. Figure 28 provides an economic analysis of the cost of manufacturing solar cell-quality silicon wafers by the Czochralski process [18].
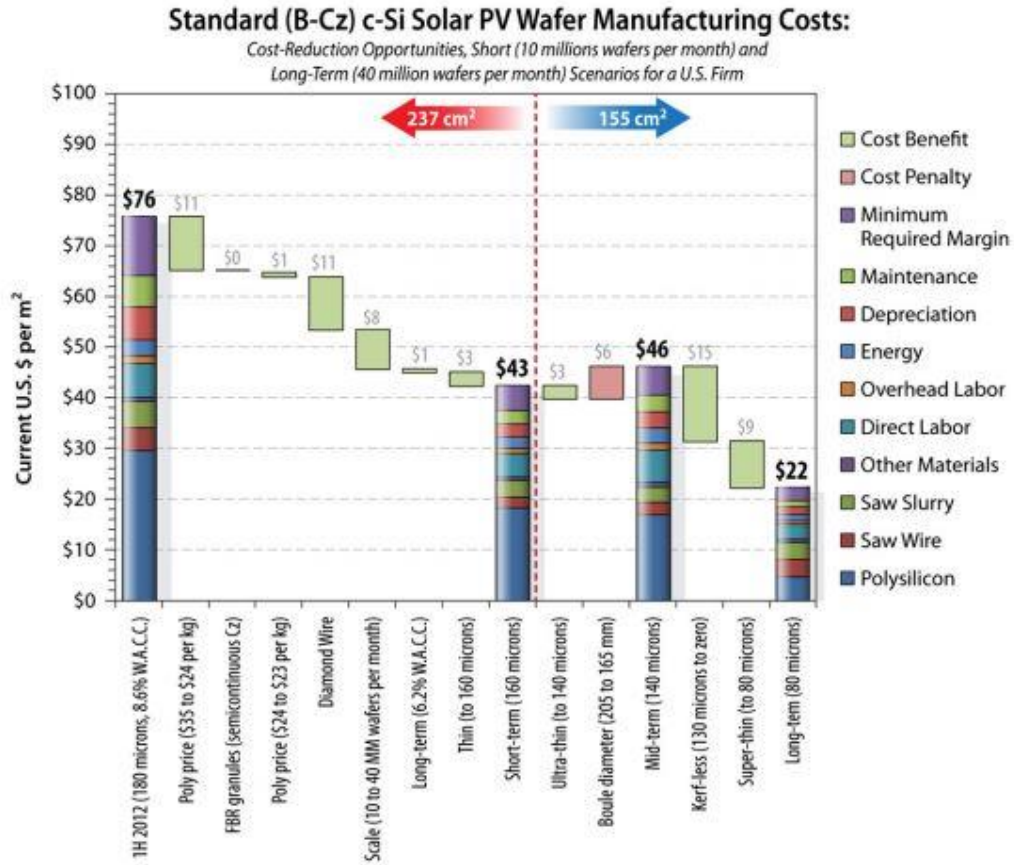
Figure 28 - Cost analysis of the manufacture of solar cell-quality silicon wafers by the Czochralski process [18]

Since the silicon substrate accounts for nearly 99% of the bulk of the tandem cell, it also accounts for a significant portion of the material and production costs of the tandem cell. The bar in the center marked "short-term" represents the cost of production for a 160 micron thick PV wafer, which corresponds to the substrate needed for producing the tandem cell design. The approximated cost for producing and processing is $43 per m^2. The cost of tellurium, as of 2012, is approximately $0.034 per Watt peak when processed for photovoltaic applications [19].

A cost analysis for the price of CdTe/Si cell production was performed by Tamboli, et al [10] using the cost assumptions above and is summarized in Figure 29.
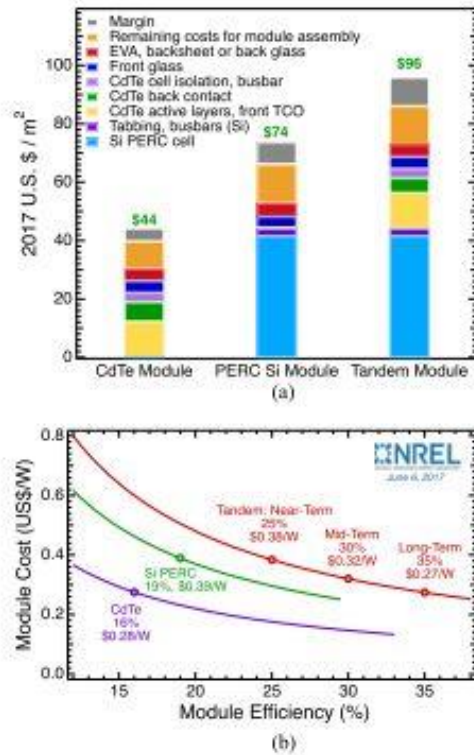
Figure 29 - Economic analysis of CdTe/Si PV Module manufacture

Their projected cost of a CdTe/Si solar cell module is $96 per m^2. With a simulated maximum efficiency of 27.19% under an illumination of 1000 W/m^2, the tandem cell design is capable of producing 271.9 W/m^2. At a cost of $96/m^2, this corresponds to a projected production cost of $0.35/W. For a 527 W nominal cell (standard industrial size of 39 in. x 77 in.), the cost is approximately $186 for a single cell material and processing. As of 2016, a standard-efficiency crystalline silicon solar cell cost of production is $0.50/W [20]. In order to manufacture a cell that can produce 527 W, the cell area would have to be 42.8% larger than the standard commercial cell and would cost $263.50, $77.50 more than the production of a tandem CdTe-Si solar cell. In other terms, the proposed tandem cell design is only a 42.8% cost increase over a standard silicon solar cell.

Figure 30 depicts the cost per Watt breakdown against multiples of the production cost of a standard silicon solar cell.
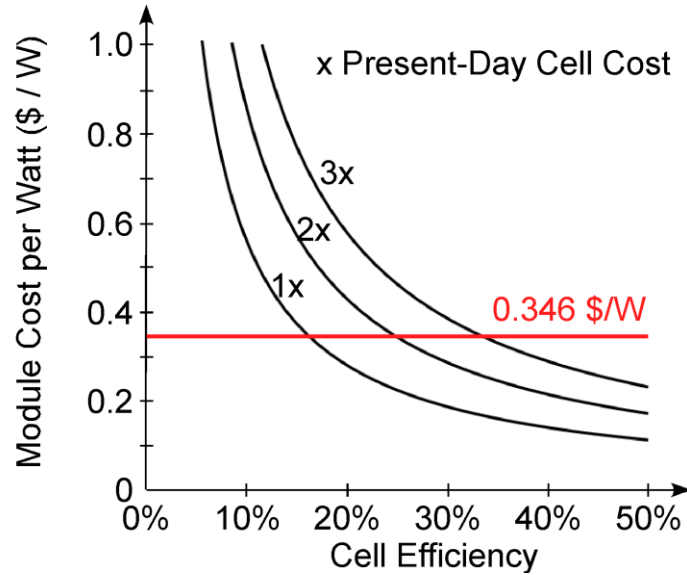
Figure 30 - Multiples of the standard silicon solar cell cost per Watt against increasing nominal cell efficiencies [21]

The key conclusion to draw from this figure is the bisection of the horizontal module cost line and the 2x curve. If the cost of producing a solar cell were to double, due to the increased material and processing costs of the tandem cell design, it would need to exceed 24.8% efficiency to be cost-justified [21]. The CdTe/Si tandem design presented in this paper represented a 42.8% cost increase over a standard silicon cell, well below the doubling threshold, and also exceeded the 24.8% efficiency mark by nearly 3%.

6. **Conclusion**

The proposed design for a CdTe-Si tandem solar cell yields a simulated efficiency in excess of 27% under an AM1.5 spectrum, well over 10% greater than that of a standard

industrial single-junction silicon cell [3]. The four junction design requires slightly more material in the form of a ZnO separator layer and more wire tracing to connect to an inverter, as well as a more elaborate inverter, but allows the CdTe absorber layers and Si absorber layers to be optimized separately, without the need to sacrifice efficiency in order to match current outputs. The features that make this design advantageous are:

1. The sub-cells are electrically separated to essentially act as two individual band-gap matched photovoltaic units, but the mechanical stacking reduces the overall footprint required.

2. By using ZnO as a mechanical separator, the cell can be made without the more traditional Indium Tin Oxide (ITO) TCO layer, which is acidic and degrades cell performance over time.

3. The mechanical separation of the CdTe and Si allows the CdTe to be grown by epitaxy on the ZnO without concern for the material strain caused by the lattice constant mismatch of the CdTe and Si.

4. The use of CdTe as the large band-gap semiconductor promotes high cell efficiency in the visible light portion of the solar radiation spectrum with the application of optically thin (100 nm) absorber layers.

5. The Si cell, which contributes a lower level of current to the overall cell output because of the high efficiency of optical absorption in the CdTe cell, still offers a mechanically strong and stable substrate for supporting the ZnO and CdTe layers.

At this considerably high conversion efficiency, it is possible to reduce the cost of production on a per-Watt basis from $0.50/W for a standard silicon heterojunction cell to approximately $0.35/W for the tandem design. The tandem design also reduces the required land footprint to

produce a nominal amount of power by 42.8%. This means that the CdTe-Si tandem design is viable for both utility-level application and for rooftop installations on private residences and businesses. The application of angular surface geometries to redirect light and increase photon mean path length could increase the overall efficiency, particularly in the Si sub-cell, and make this tandem design more cost-competitive with other forms of renewable energy.

7. References

[1] U.S. Department of Energy *Soft Costs Factsheet*. 2018.
https://energy.gov/sites/prod/files/2016/05/f32/SC%20Fact%20Sheet-508.pdf

[2] U.S. Department of Energy Solar Energy Technologies Office. *Concentrating Solar Power*. 2018. https://energy.gov/eere/solar/concentrating-solar-power

[3] Vikram Aggarwal. "What are the most efficient solar panels on the market?". *EnergySage.* 2018. https://news.energysage.com/what-are-the-most-efficient-solar-panels-on-the-market/

[4] Thue Trofod Larsen-Olsen. "Tandem Solar Cells". *DTU Energy.* 2017. <http://plasticphotovoltaics.org/lc/lc-polymersolarcells/lc-tandem.html>

[5] Russell Jones, James Ermer, Christopher Fetzer and Richard King. "Evolution of Multijunction Solar Cell Technology for Concentrating Photovoltaics". *Japanese Journal of Applied Physics.* Vol 51. 2012.
http://www.spectrolab.com/pv/support/Evolution_of_Multijunction_Solar_Cell_Technology_for_Concentrating_Photovoltaics.pdf

[6] Y. Tawada, H. Okamoto and Y. Hamakawa. "a-SiC:H/a-Si:H heterojunction solar cell having more than 7.1 % conversion efficiency". *Appl. Phys. Lett.* 39, 237. 1981. Doi: 10.1063/1.92692.

[7] Vinay Budhraja, Durga Misra and N.M. Ravindra. "Advancements in PV Multicrystalline Silicon Solar Cells from 1980 to 2010 – An Overview". IEEE. 2011.

[8] M.F. Lamorte and D. Abbott. "Two-Junction Cascade Solar Cell Characteristics under 10^3 Concentration Ratio and AM0-AM5 Spectral Conditions". *Conference Record of the IEEE Photovoltaic Specialists Conference*, pg 874-880, 1978.

[9] Sabina Abdul Hadi, Eugene A. Fitzgerald, Steven A. Griffiths, and Ammar Nayfeh. "III-V/Si Dual Junction Solar Cell at scale: Manufacturing costs for step-cell based technology". *Journal of Renewable and Sustainable Energy* 10, 015905, 2018.

[10] Adele C. Tamboli, David C. Bobela, Ana Kanevce, Timothy Remo, Kirstin Alberi and Michael Woodhouse. "Low Cost CdTe/Si Tandem Solar Cells". *IEEE Journal of Photovoltaics*, Vol. 7, No. 6. November 2017.

[11] C.G. Fonstad. "Lecture 1 - The Compound Semiconductor Pallette". MIT Lecture. https://ocw.mit.edu/courses/electrical-engineering-and-computer-science/6-772-compound-semiconductor-devices-spring-2003/lecture-notes/Lecture1v2.pdf

[12] Corsin Battaglia, Andres Cuevas and Stefaan de Wolf. "High-Efficiency Crystalline Solar Cells: Status and Perspectives". *Energy Environ. Sci.*, Vol 9, 1552, 2016.

[13] Darius Kuciauskas, Ana Kanevce, Pat Dippo, Shahram Seyedmohammadi and Roger Malik. "Minority-Carrier Lifetime and Surface Recombination Velocity in Single-Crystal CdTe". *IEEE Journal of Photovoltaics*, Vol 5, No 1. January 2015.

[14] Xiaoqin Ding and Yunfeng Lai. "Electrical and Optical Properties of Zinc Oxide Thin Films Deposited by Magnetron Sputtering". *ECS Transactions*, 34 (1) 577-582. 2011.

[15] *American Society for Testing and Materials (ASTM) Terrestrial Reference Spectra for Photovoltaic Performance Evaluation*. National Renewable Energy Laboratories (NREL). 2003. Online. http://rredc.nrel.gov/solar/spectra/am1.5/

[16] Shamus McNamara. *Operating Principles of Semiconductor Devices*. University of Louisville. Print. 2016.

[17] Sheng Li. *Semiconductor Physical Electronics (2nd Ed)*. Springer-Verlag New York City, NY. 2006. Print.

[18] Alan Goodrich, et al. "A wafer-based monocrystalline silicon photovoltaics road map: Utilizing known technology improvement opportunities for further reductions in manufacturing costs". *Solar Energy Mater and Solar Cells*. 114. 2013.

[19] Mike Redlinger, Martin Lokanc, Roderick Eggert, Michael Woodhouse and Alan Goodrich. "The Present, Mid-Term, and Long-Term Supply Curves for Tellurium; and updates in the results from NREL's CdTe PV Module Manufacturing Cost Model". National Renewable Energy Laboratory. 2013. Online. https://www.nrel.gov/docs/fy13osti/60430.pdf

[20] Atse Louwen, Wilfried Van Sark, Ruud Schropp, Andre Faaij. "A cost roadmap for silicon heterojunction solar cells". *Solar Energy Mater and Solar Cells.* 147. 2016.

[21] Dr. Shamus McNamara. "Cost Analysis for Photovoltaic Cell Efficiency".University of Louisville Micro/Nano Technology Center. Presentation. 2018.

7. Appendix

i. Silvaco Code

#Written by Jacob Vittitow, Fall 2017

#Silicon defect definitions and IV simulation commands based on solarex12.in

#CdTe Parameters are as defined in Atlas User's Manual V 5.18.3, Appendix B

go atlas

Structure Generation

mesh space.mult=1.2

x.m l=0 s=.50

x.m l=10 s=.50

y.m l=0.0 s=0.01

y.m l=0.1 s=0.01

y.m l=0.2 s=0.01

y.m l=0.3 s=0.01

y.m l=0.350 s=0.01

y.m l=0.500 s=0.01

y.m l=0.55 s=0.01

y.m l=0.60 s=0.01

y.m l=1.60 s=0.2

y.m l=150.555 s=0.002

y.m l=150.6 s=0.2

y.m l=152.6 s=0.2

#top cell: CdTe PN Junction Number 1

region num=1 mat=CdTe x.min=0 x.max=10 y.min=0.1 y.max=0.2 name=CdTeN

region num=2 mat=CdTe x.min=0 x.max=10 y.min=0.2 y.max=0.3 name=CdTeP

#bottom cell: Si PN Junction Number 2

region num=3 mat=silicon x.min=0 x.max=10 y.min=0.60 y.max=1.6 name=SiN

region num=4 mat=silicon x.min=0 x.max=10 y.min=1.6 y.max=150.555 name=SiP

region num=5 mat=ZnO x.min=0 x.max=10 y.min=0.350 y.max=0.500 name=Buffer

region num=6 mat=silicon x.min=0 x.max=10 y.min=150.555 y.max=150.6 name=SiAlContact

region num=7 mat=silicon x.min=0 x.max=10 y.min=0.55 y.max=0.60 name=SiZnOContact

elec num=1 name=cathode x.min=0 x.max=10 y.min=0 y.max=0.1 mat=ZnO

elec num=2 name=anode x.min=0 x.max=10 y.min=150.6 y.max=152.6 mat=Aluminum

#p-type ZnO to act as anode of top cell - buffer layer

elec num=3 name=comP x.min=0 x.max=10 y.min=0.300 y.max=0.350 mat=ZnO

elec num=4 name=comN x.min=0 x.max=10 y.min=0.500 y.max=0.550 mat=ZnO

doping uniform conc=1e15 phosphorus region=1

#n-doped CdTe

doping uniform conc=1e15 boron region=2

#p-doped CdTe

doping uniform conc=1e17 phosphorus region=3

#n-doped Si

doping uniform conc=1e16 boron region=4

#p-doped Si

doping uniform conc=2e18 boron region=6

#heavily doped p region to ensure good ohmic contact between the Al anode and the p-Si region

doping uniform conc=1e19 phosphorus region=7

#heavily doped n region to ensure good ohmic contact between the ZnO ComN and the N-Si region

doping uniform conc=1e20 phosphorus name=cathode

doping uniform conc=1e20 phosphorus name=comN

doping uniform conc=6e21 aluminum name=comP

#doped ZnO cathode for good ohmic contact - doping with Aluminum improves transmission of light in the visible range and raises bandgap to reduce parasitic light absorption

#An aluminum doping conc of 6e21 corresponds to 3 weight percent Al in ZnO, which the literature suggests is the proportion with the highest conductivity

#Carrier lifetimes of CdTe and Si based on Literature (see Vittitow Folder)

material taun0=333e-9 taup0=333e-9 sopra=Cdte.nk region=1

material taun0=333e-9 taup0=333e-9 sopra=Cdte.nk region=2

IV Simulation

#Simulation temp of 300K (27 degC)

#consrh - Shockley-Read-Hall Recombination Model

#conmob - carrier mobility in Si varies with doping concentration (only valid for 300K)

models consrh conmob fermi auger bgn print temp=300

#Set y-origin to negative number to allow beam to spread to cover entire solar cell

#back.refl accounts for light reflection at the Aluminum anode interface

beam num=1 x.orig=5.0 y.orig=-5.0 min.window=-5.0 max.window=5.0 angle=90 AM1.5
wavel.num=150 verbose back.refl reflects=1

method maxtrap=10

output opt.int band.temp

solve init

save outf=CdTeTandem_outputnolight.str

output charge opt.intens

solve b1=1

save outf=CdTeTandem_outputwithlight.str

tonyplot CdTeTandem_outputnolight.str

tonyplot CdTeTandem_outputwithlight.str

log outf=CdTeTandemTopCell_output.log

output charge opt.intens

solve vanode=0.0 name=comP vstep=0.01 vfinal=0.85 beam=1

log off

log outf=CdTeTandemBottomCell_output.log

output charge opt.intens

solve v4=0 v3=0 vcathode=0 vanode=0.0 name=anode vstep=0.01 vfinal=0.55 beam=1

log off

tonyplot CdTeTandemTopCell_output.log

tonyplot CdTeTandemBottomCell_output.log

#Command generates a solar cell efficiency vs wavelength curve with the wavelength varying from 300 nm to 1.25 um

SOLAR IW=CdTeTandem_EfficiencyVWavelength min.wave=0.300 max.wave=0.800 step.wave=0.05

#tonyplot CdTeTandem_EfficiencyVWavelength

extract init infile="CdTeTandemTopCell_output.log"

extract name="Jsc" y.val from curve(v."comP", i."comP") where x.val=0.0

extract name="Voc" x.val from curve(v."comP", i."comP") where y.val=0.0

extract name="Pm" min(curve(v."comP", (v."comP" * i."comP")))

extract name="Vm" x.val from curve(v."comP", (v."comP"*i."comP")) \

        where y.val=$"Pm"

extract name="Im" $"Pm"/$"Vm"

extract name="FF" $"Pm"/($"Jsc"*$"Voc")

extract name="Eff%" 1e13*$Pm/1000*-1

extract init infile="CdTeTandemBottomCell_output.log"

extract name="Jsc" y.val from curve(v."anode", i."anode") where x.val=0.0

extract name="Voc" x.val from curve(v."anode", i."anode") where y.val=0.0

extract name="Pm" min(curve(v."anode", (v."anode" * i."anode")))

extract name="Vm" x.val from curve(v."anode", (v."anode"*i."anode")) \

       where y.val=$"Pm"

extract name="Im" $"Pm"/$"Vm"

extract name="FF" $"Pm"/($"Jsc"*$"Voc")

extract name="Eff%" 1e13*$Pm/1000*-1